

Analysis of Mercury Coordination Environments of Tridentate and
Tetradentate Nitrogen Based Ligands by NMR Spectroscopy and
X-Ray Crystallography

A Thesis

Presented to

The Faculty of the Department of Chemistry

The College of William & Mary in Virginia

In Partial Fulfillment

Of the Requirements for the Degree of

Master of Arts

by

Rachel Freer

1997

APPROVAL SHEET


This thesis is submitted in partial fulfillment
of the requirements for the degree of

Master of Arts




Author

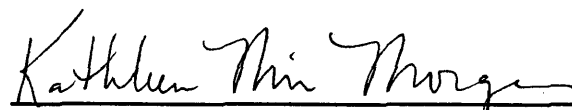
Approved, August 1997



Deborah C. Bebout



Robert A. Orwoll



Kathleen M. Morgan

TABLE OF CONTENTS

ACKNOWLEDGEMENTS.....	iv
LIST OF TABLES.....	v
LIST OF FIGURES.....	vi
ABSTRACT.....	vii
INTRODUCTION.....	2
EXPERIMENTAL.....	9
RESULTS AND DISCUSSIONS.....	15
I. Organic Synthesis.....	15
II. X-Ray Diffraction Analysis Studies.....	16
Crystal Structure of [Hg(BEPA)](ClO ₄) ₂	16
Crystal Structure of [Hg(BEPA)Cl ₂].....	17
Discussion of Crystal Structures.....	18
III. NMR Solution-State Studies of Hg(II) Coordination.....	21
Solution-State Investigations of BEPA Coordination to Hg(II).....	23
Solution-State Investigations of TEPA Coordination to Hg(II).....	30
CONCLUSION.....	33
REFERENCES.....	36
APPENDIX.....	40
VITA.....	64

ACKNOWLEDGEMENTS

I would like to especially thank Dr. Bebout for her guidance and encouragement during the course of this research project. In addition the research of Caryn Prairie, presented in her 1995 Honors thesis, provided a foundation upon which this present research has built upon. I would also like to thank the other members of the laboratory group, Jon, Dave, Kristi, Katie, Sagar, Anne, and Jim for providing assistance throughout the last two years. Finally, I would like to thank my family, the Joyners, and Chris whose love and support motivated this accomplishment.

LIST OF TABLES

Table		Page
1	Selected crystallographic data for [Hg(BEPA)](ClO ₄) ₂ .	45
2	Atomic coordinates and equivalent isotropic displacement parameters for [Hg(BEPA)](ClO ₄) ₂ .	46
3	Bond Lengths (Å) for [Hg(BEPA)](ClO ₄) ₂ .	47
4	Bond Angles (°) for [Hg(BEPA)](ClO ₄) ₂ .	47
5	Anisotropic displacement parameters for [Hg(BEPA)](ClO ₄) ₂ .	48
6	Hydrogen coordinates and isotropic displacement parameters for [Hg(BEPA)](ClO ₄) ₂ .	49
7	Selected crystallographic data for [Hg(BEPA)Cl ₂].	51
8	Atomic coordinates and equivalent isotropic displacement parameters for [Hg(BEPA)Cl ₂].	52
9	Bond Lengths (Å) for [Hg(BEPA)Cl ₂].	52
10	Bond Angles (°) for [Hg(BEPA)Cl ₂].	53
11	Anisotropic displacement parameters for [Hg(BEPA)Cl ₂].	53
12	Hydrogen coordinates and isotropic displacement parameters for [Hg(BEPA)Cl ₂].	54

LIST OF FIGURES

Figure		Page
1	BEPA and TEPA	8
2	Synthesis of BEPA and TEPA	15
3	Thermal ellipsoid representation of $[\text{Hg}(\text{BEPA})](\text{ClO}_4)_2$.	50
4	Thermal ellipsoid representation of $[\text{Hg}(\text{BEPA})\text{Cl}_2]$.	55
5	The chemical shifts of protons of BEPA as a function of the $\text{Hg}(\text{ClO}_4)_2$ to BEPA ratio in CD_3CN at 20°C .	56
6	The chemical shifts of protons of BEPA as a function of the HgCl_2 to BEPA ratio in CD_3CN at 20°C .	57
7	Proton NMR spectra recorded at select ratios of $\text{Hg}(\text{ClO}_4)_2$ to BEPA.	58
8	Proton NMR spectra recorded at select ratios of HgCl_2 to BEPA.	59
9	Proposed 1:2 complexes for $[\text{Hg}(\text{BEPA})]^{2+}$.	26
10	The chemical shifts of protons of TEPA as a function of the $\text{Hg}(\text{ClO}_4)_2$ to TEPA ratio in CD_3CN at 20°C .	60
11	The chemical shifts of protons of TEPA as a function of the HgCl_2 to TEPA ratio in CD_3CN at 20°C .	61
12	Proton NMR spectra recorded at select ratios of $\text{Hg}(\text{ClO}_4)_2$ to TEPA.	62
13	Proton NMR spectra recorded at select ratios of HgCl_2 to TEPA.	63
14	Proposed structure for $[\text{Hg}(\text{TEPA})_2](\text{ClO}_4)_2$.	31
15	Ligands to be examined in future studies	35

ABSTRACT

The dynamics of Hg(II) coordination by the potentially tridentate ligand bis-2-(2-pyridylethyl)amine (BEPA) and potentially tetradentate ligand tris(2-pyridylethyl)amine (TEPA) were examined by solution-state NMR and X-Ray crystallography. Deuterated acetonitrile solutions containing metal-to-ligand stoichiometries of 0.125 to 3.0 were examined. Mercury coordination complexes exhibiting rarely observed room temperature solution-state NMR $^1\text{H}^{199}\text{Hg}$ and $^{13}\text{C}^{199}\text{Hg}$ satellites were characterized. The effects of counter ion, concentration and temperature on the solution-state NMR properties were investigated. Solid-state structures obtained by X-Ray crystallography were correlated with the solution-state NMR data. The six-coordinate complex $[\text{Hg}(\text{BEPA})](\text{ClO}_4)_2$ (**1**) crystallizes in the monoclinic Space Group $P\bar{1}$ with $a = 10.950(3)$ Å, $b = 12.826(4)$ Å, $c = 13.035(4)$ Å, $\alpha = 67.39(2)^\circ$, $\beta = 82.74(2)^\circ$, and $\gamma = 68.09(2)^\circ$ with $Z = 2$. The complex is tridentate with a Hg- N_{amine} distance of 2.510(8) Å and Hg- N_{pyridyl} distances of 2.104(6) Å and 2.114(6) Å. Close contact from three perchlorates completes a pseudo-octahedral environment. The five-coordinate complex $[\text{Hg}(\text{BEPA})\text{Cl}_2]$ (**2**) crystallizes in the orthorhombic Space Group $Pnma$ with $a = 13.424(3)$ Å, $b = 14.854(3)$ Å, and $c = 8.118(2)$ Å with $Z = 4$. $[\text{Hg}(\text{BEPA})\text{Cl}_2]$ exhibits distorted trigonal bipyrimid geometry with a Hg- N_{amine} bond distance of 2.289 Å and Hg- N_{pyridyl} distances of 2.549(16) Å. Structural characterization of a complex of TEPA is in progress.

Analysis of Mercury Coordination Environments of Tridentate and
Tetradentate Nitrogen Based Ligands by NMR Spectroscopy and X-Ray
Crystallography

INTRODUCTION

An estimated 30% of all proteins require interactions with a metal ion for full physiological activity.¹ Understanding the chemical and structural nature of the metal coordination site of metalloproteins is essential to understanding their biological function. Detailed elucidation of subtle structural differences in metal binding sites will help provide information as to the precise processes used in diverse roles, such as catalysis, electron transport, and gene regulation.²

Formation of a biologically active protein requires that its polypeptide chain be folded into an appropriate three-dimensional conformation. Therefore, it is not surprising that a major goal of biochemical research is to understand the specific interactions that allow proteins to fold and perform their biological role. A knowledge of the various levels of protein structure, especially amino acid sequence and three-dimensional spatial configuration is essential to answering these questions. Over thirty years ago, Anfinsen and his colleagues proposed that the linear sequence of amino acids determines the final three-dimensional folded structure of a protein.³ Through advances in sequencing technology, primary structure is determinable for most proteins, however, the mechanism of protein folding still remains a mystery. Interestingly, polypeptide chains can adopt an extremely large number of conformations, an average of 10 conformations per amino acid residue. On a practical time scale, it is not feasible for a protein to try out all of its conformations before arriving at its final native structure. For example, if a polypeptide chain of 100 residues has 10^{100} possible conformations, and if it converts one conformation into another in the shortest possible time (i.e., perhaps 10^{-13} s), the average time required to sample all possible conformations would be 10^{77} years.⁴ Nevertheless,

proteins are observed to fold in 10^{-1} to 10^3 s both in vivo and in vitro. This observation leads to the conclusion that proteins do not fold by sampling all of the possible conformations randomly until the one with the lowest free energy is found. In order for protein folding to occur on such a short time scale, the folding process must be directed in some way. Many metal ion binding sites are located on the interior of proteins, suggesting an important role for metal ions in the thermodynamic stabilization of protein folding intermediates. In fact, it has been shown that metalloprotein folding slows by up to three orders of magnitude in the presence of metal chelators.⁵

Furthermore, the single native structure of a protein is not necessarily the most thermodynamically stable form. Kinetic accessibility to isomeric structures, which is influenced by partial folding of the incomplete polypeptide during synthesis or involvement with other molecules such as molecular chaperone proteins must also be considered. Metalloprotein folding intermediates are likely to be stabilized in part by the strong coordinate covalent and ionic bonds that form between the amino acids of peptides and metal ions.

Common experimental approaches to measuring the rates of protein folding and unfolding include intrinsic fluorescence, absorbance and circular dichroism.⁷ A drawback to these techniques is their inability to provide specific information about the structure of protein folding and unfolding intermediates. Other studies used hydrogen-deuterium exchange combined with multidimensional proton NMR spectroscopy to identify specific regions of secondary structure formed during the folding process.^{8,9,10} This technique, by monitoring rates of amide proton exchange, provides detailed and specific information about the behavior of the backbone of the protein and the formation

of secondary structure, but does not, in general, monitor side chain environment.^{7,11}

Stopped-flow NMR has recently been applied to the real-time investigation of protein unfolding and refolding.^{5,11} This experiment allowed a direct, real-time measurement of the environment of side chains in different regions of the protein to be examined as a function of time. The ability of NMR to detect through bond coupling gives the technique enormous potential for monitoring interactions between specific atoms during a kinetic process. However, structural information about the formation of specific regions of tertiary structure and about the behavior of side chains during the folding process is still limited.

There have been many approaches towards elucidating the nature and geometry of the immediate coordination sphere around a metal ion, and although X-ray diffraction methods yield the most indisputable results, many metalloproteins have not yet succumbed to this technique. X-ray crystallography is a complicated technique and not readily applicable to complex molecules such as metalloproteins. Successful interpretation of three-dimensional structure by x-ray crystallography requires large, individual, well-ordered crystals of the protein to be analyzed. Proteins are inherently designed to function in solution or membranes and not to form crystals. Thus, it is often extremely difficult to grow regular crystals of proteins. Recently, the technique of high resolution nuclear magnetic resonance (NMR) spectroscopy has been used to study metal coordination in a variety of metalloproteins. Specific ligating protein groups surround the metal ion in the active site of metalloproteins. These simultaneous, cooperative interactions lead to considerable metal specificity. Cass and associates¹² have proposed that an ideal probe of metal coordination would involve the use of a metal ion which

would monitor interactions between the metal and associated ligands directly through bonds. A metal ion with a nuclear spin $I = \frac{1}{2}$ is expected to be such a probe because heteronuclear coupling to the NMR active nuclei of the protein can be detected by NMR spectroscopy. Unfortunately, none of the metals commonly found in metalloproteins possess favorable NMR properties. The only nonradioactive, preferred spin $\frac{1}{2}$ metal nuclei with natural abundance and receptivity adequate for these types of investigations are ^{103}Rh , ^{107}Ag , ^{109}Ag , ^{111}Cd , ^{113}Cd , ^{196}Pt and ^{199}Hg .

In analogy to well established ^{113}Cd studies, ^{199}Hg could prove to be a powerful probe of the three-dimensional ligand environment provided by metal binding sites in metalloproteins. The ability of Hg to form exceptionally strong bonds with N- and S-donor ligands and to form complexes with a wide variety of conformations and ligand numbers will facilitate development of ^{199}Hg as a metallobioprobe. The 5000 parts per million (ppm) chemical shift range of ^{199}Hg is significantly greater than that of ^{113}Cd . As a result, the chemical shift of ^{199}Hg is extremely sensitive to the number and identity of bound ligands as well as coordination geometry. ^{199}Hg has a natural abundance of 16.8% and a receptivity 5.4 times greater than ^{13}C .¹⁴ Most significantly, ^{199}Hg ions have been found to readily replace various native transition metal ions with preservation of the metal coordination sphere and very limited changes in overall protein structure. For example, replacement of the Cu(II) atom in plastocyanin by Hg(II) caused only minor changes in the geometry of the metal site, and there were few significant changes elsewhere in the molecule.¹⁵ In fact, the irregular, quasi-tetrahedral coordination geometry found in Cu(II)-plastocyanin remained virtually unchanged in Hg(II)-plastocyanin, apart from a

slight enlargement of the coordination polyhedron required to accommodate the mercury atom.

More recently, Blake and associates demonstrated that substitution of the native Fe(II) in the protein *P. Furiosus* rubredoxin by Zn(II), Hg(II) or Cd(II) does not lead to a measurable structural perturbation.² To gain further insight into the structural and chemical nature of the metal coordination site, detailed multidimensional NMR studies were initiated on the ¹⁹⁹Hg- and ¹¹³Cd- substituted proteins. These experiments confirmed that substitution by ¹⁹⁹Hg⁺² and ¹¹³Cd⁺² does not alter the globular structure of the protein. In addition, NMR analysis established that metal substitution does not significantly change the conformation of the metal binding residues. Two-dimensional heteronuclear multiple quantum coherence (HMQC) NMR studies were used to evaluate the metal chemical shifts and identify protons of amino acids that exhibited scalar coupling to the metals. The ¹H-¹⁹⁹Hg HMQC NMR method is applicable to proteins that contain metal sites with high symmetry (the metal site of rubredoxins exhibits T_d symmetry). Severe chemical shift anisotropy has been observed for mercury sites with reduced symmetry, leading to broadening of the ¹⁹⁹Hg signal in such proteins. Blake's study represents the first application of ¹⁹⁹Hg HMQC spectroscopy to metalloproteins, and provides ¹⁹⁹Hg-metalloprotein chemical shift information that may be useful for evaluating the ¹⁹⁹Hg spectra of other mercury-substituted proteins.

NMR spectroscopy has proven to be a powerful probe in the investigation of metal coordination sites due to its ability to detect direct, through bond effects between the metal ion and the surrounding ligand environment. Investigations of the coordination chemistry of ¹⁹⁹Hg is complicated by its tendency to form complexes with many different

coordination numbers and geometries. Despite the high thermodynamic stability of Hg(II) complexes, numerous studies have demonstrated that Hg(II) is prone to rapid exchange among ligating groups in solution¹⁶ As a result, observations of satellites attributable to proton or carbon coupling to the $I = 1/2$, 16.85% natural abundance ¹⁹⁹Hg nucleus has been rare for Hg(II) coordination compounds in solution.^{12,17} Mercury has only one other NMR active isotope, ²⁰¹Hg, and the large quadrupole moment of this nucleus prevents routine observation. Recent investigations of Hg(II)-substituted proteins have demonstrated that the multidentate coordination environment of proteins can establish slow exchange conditions sufficient for observation of ¹H¹⁹⁹Hg coupling by solution-state NMR methods.^{2,12,14} In order to further examine these phenomena, we have begun to investigate the Hg(II) coordination chemistry of a series of polydentate ligands. Polydentate ligands were selected based on their ability to geometrically and entropically restrict the number of accessible structures, although to a lesser degree than the well defined metal binding sites of proteins.

Currently, structural and donor atom predictions of metal coordination environments in mercury-substituted proteins are based mainly on correlations with spectra obtained for model compounds, and to a lesser extent, for proteins with known structure. As such, any new information regarding the ¹⁹⁹Hg chemical shift of mercury substituted proteins is useful. The long term goal of this research is to add to the existing knowledge of ¹⁹⁹Hg chemical shift and coupling constant data through the solution-state NMR investigations of dipodal and tripodal, nitrogen-containing ligands that model protein metal-binding sites that contain histidine. Tripodal ligands have been applied extensively to the synthesis of metal complexes because of their ease of preparation,

wealth of spectroscopic data and X-ray crystallographic data available for their metal complexes, and the predictable changes in the physical properties of the metal complex with variation in the ligand.¹⁷ We have characterized coordination and exchange dynamics of these ligands with ^{199}Hg through solution-state NMR studies.

The potentially tridentate bis(2-pyridylethyl)amine (BEPA) and potentially tetradentate tris(2-pyridylethyl)amine (TEPA) ligands were chosen for this study because their pyridine rings model protein ligation by histidine. The ligands are composed of a central amine nitrogen bound by ethyl bridges to two and three pyridyl rings, as shown in the figure below.

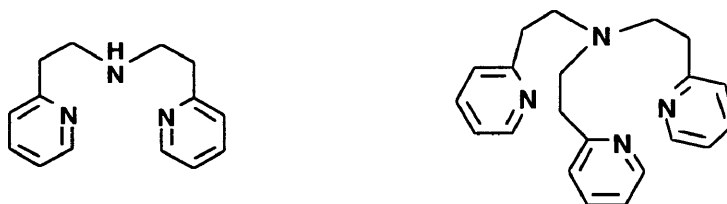


Figure 1. *BEPA and TEPA*

This work describes the synthesis and characterization of BEPA and TEPA as well as NMR investigations of the exchange dynamics of these complexes with Hg(II) in solution. Solution studies of $[\text{Hg}(\text{BEPA})](\text{ClO}_4)_2$ and $[\text{Hg}(\text{BEPA})\text{Cl}_2]$ in deuterated acetonitrile were correlated with solid-state structures determined by X-ray diffraction. The synthesis and characterization of $[\text{Hg}(\text{TEPA})](\text{ClO}_4)_2$ is reported and determination of the crystal structure is pending. The apparent solution equilibria are discussed, including analysis of observed $^1\text{H}^{199}\text{Hg}$ and $^{13}\text{C}^{199}\text{Hg}$ coupling.

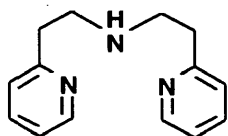
EXPERIMENTAL

Methods and Materials. Starting materials were of commercially available reagent quality unless otherwise stated. All synthetic procedures were conducted under a flow of argon. Chromatographic separations were performed using thin layer chromatography (TLC) on alumina plates, visualized by iodine staining and alumina column chromatography methods.

FT-IR spectra of crystals and liquids were recorded in KBr pellets and thin films on a Perkin Elmer 1600. Mass spectrometry analyses were performed on a Hewlett Packard 5890 Series II Gas chromatograph with a Hewlett Packard 5971A Mass Selective Detector. Elemental analyses were carried out by Atlantic Microlab, Inc., Norcross, Georgia.

All of the perchlorate salts of mercury (II) complexes included in this work were stable for routine synthesis and purification procedures. However, caution should be exercised because perchlorated salts of metal complexes with organic ligands are potentially explosive.¹⁸

Synthesis of bis(pyridylethyl)amine (BEPA).¹⁹ Methanol (100 mL) was added



F.W. 227.31

to a 250 mL round bottom flask, followed by freshly distilled 2-

vinylpyridine (10.8 mL, 0.100 moles), and freshly distilled 2-(2-

aminoethyl)pyridine (11.9 mL, 0.100 moles). The flask was put in an

ice bath for 10 minutes followed by the slow addition of glacial

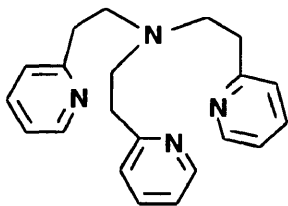
acetic acid (5.7 mL, 0.100 moles). The clear colorless mixture was heated to reflux for

24 hours under argon yielding a pale yellow solution. The methanol was removed by rotary evaporation, leaving a viscous, pale yellow oil. The flask was put in an ice bath and deionized water (20 mL) was added. The solution was allowed to chill for 10 minutes and then 30% NaOH (3 mL) was slowly added to neutralize the solution. The solution was transferred to a 250 mL separatory funnel and extracted with four 25 mL portions of chloroform until the organic layer was colorless. The combined organics were dried over MgSO_4 , filtered into a 50 mL round bottom, and the chloroform was removed by rotary evaporation.

Unreacted 2-vinyl pyridine was removed from the crude BEPA by stirring overnight under reduced pressure (0.01 mm of Hg). Fractional distillation of the residue provided a first fraction containing 2-(2-aminoethyl)pyridine (40-45° C, 0.05 mm Hg, lit. 92-93° C), followed by bis(pyridylethyl)amine (123° C, 0.03 mm Hg) in 32.9 % yield. The final product, a colorless oil, was stored under argon at -20° C.

$^1\text{H NMR}$ (CD_3CN) (Appendix 1) : δ 2.86 (t, J = 6 Hz, 4 H_c), 2.93 (t, J = 6 Hz, 4 H_i), 7.13 (t, J = 6 Hz, 2 H_b), 7.18 (d, J = 8 Hz, 2 H_d), 7.62 (t, J = 8 Hz, 2 H_e), 8.43 (d, J = 4 Hz, 2 H_a). **$^{13}\text{C NMR}$** (CD_3CN) (Appendix 1) : δ 39.00 (C_e), 50.01 (C_i), 122.16 (C_c), 124.16 (C_b), 137.25 (C_d), 150.11 (C_a), 161.74 (C_g). **GC/MS** : (rel int) 227 (M^+ , 1.4), 135 (100), 121 (14.6), 106 (58.6), 93 (30.3), 78 (16.1), 28.1 (14.9).

Synthesis of tris(pyridylethyl)amine (TEPA).²⁰ Freshly distilled 2-(2-



F.W. 332.45

aminoethyl)pyridine (2 mL, 16.72 mmol) was added to a pressure tube, followed by freshly distilled 2-vinylpyridine (5.4 mL, 50.16 mmol) and glacial acetic acid (0.96 mL, 16.72 mmol). The

solution was put under argon and the pressure tube was sealed with a teflon cap. The clear, colorless mixture was heated to reflux for 27 hours in an oil bath at 110° C yielding a deep yellow liquid. The flask was then allowed to cool, put in an ice bath and neutralized with 1 M NaOH (4 mL). The solution was extracted with three 5 mL portions of methylene chloride until the organic layer was colorless. The combined organic layers were dried over MgSO₄ and the methylene chloride was removed by rotary evaporation.

The crude TEPA was purified using column chromatography with 75% ethyl acetate/hexanes used as the eluent. A 20x140 mm column of alumina was used for each gram of crude material. Twenty-five fractions were collected and thin layer chromatography was performed to determine which fractions contained the TEPA. The fractions containing the TEPA were pooled and the solvent removed by rotary evaporation. A pale yellow oil was collected in 47.5% yield and stored under argon at -20° C.

¹H NMR (CD₃CN) (Appendix 2) : δ 2.81 (t, J = 8 Hz, 6 H_c), 2.91 (q, J = 7 Hz, 6 H_l), 7.06 (d, J = 8 Hz, 3 H_b), 7.12 (t, J = 6 Hz, 3 H_d), 7.57 (t, J = 8 Hz, 3 H_e), 8.46 (d, J = 5 Hz, 3 H_a). ¹³C NMR (CD₃CN) (Appendix 2) : δ 37.12 (C_e), 54.93 (C_f), 122.18 (C_c), 124.44 (C_b), 137.18 (C_d), 150.27 (C_a), 162.25 (C_g). GC/MS : (rel int) 240 (M⁺, 76.1), 147 (23.7), 135 (50.2), 106 (99.0), 78 (31.0), 28 (100), 18 (9.3).

Synthesis of the Complex [Hg(BEPA)](ClO₄)₂ (1). Solid Hg(ClO₄)₂ (1.0 g, 2.0 mmol) was dissolved in acetonitrile (2.5 mL) and added with stirring to a solution of BEPA (0.5 g, 2.0 mmol) in acetonitrile (2.5 mL). The solution was filtered through celite, added to a 5 mm recrystallization tube, layered with toluene and chilled to -40°C. Colorless rectangular crystals grew in sixteen days which were suitable for X-ray diffraction analysis. The crystals were found to decompose between 160-170°C.

¹H NMR (CD₃CN) (Appendix 3) : δ 3.25 (m, 4 H_c and 4 H_r), 7.71 (d, J = 8 Hz, 2 H_d), 7.80 (t, J = 6 Hz, 2 H_b), 8.20 (t, J = 8 Hz, 2 H_c), 8.74 (d, J = 5 Hz, 2 H_a). ¹³C NMR (CD₃CN) (Appendix 3) : δ 37.38 (C_e), 49.89 (C_r), 126.00 (C_c), 128.40 (C_b), 134.34 (C_d), 151.01 (C_a), 162.51 (C_g). **Analysis:** Calculate for C₁₄H₁₇Cl₂HgN₃O₈ : C, 26.83; H, 2.73; N, 6.70. Found : C, 26.89; H, 2.73; N, 6.79.

Synthesis of the Complex [Hg(BEPA)Cl₂] (2). Solid HgCl₂ (0.3 g, 1.105 mmol) was dissolved in acetonitrile (2 mL) and added with stirring to a solution of BEPA (0.25 g, 1.105 mmol) in acetonitrile (2 mL). The solution was filtered through celite, added to a 5 mm recrystallization tube, layered with 40% ethyl acetate/hexane and chilled to -40°C. Colorless rectangular crystals grew in four days which were suitable for X-ray diffraction analysis. The crystals were found to have a melting point range of 109-111°C.

¹H NMR (CD₃CN) (Appendix 4) : δ 3.18 (m, 4 H_c), 3.19 (m, 4 H_r), 7.33 (d, J = 8 Hz, 2 H_d), 7.37 (t, J = 5 Hz, 2 H_b), 7.80 (t, J = 8 Hz, 2 H_c), 8.58 (d, J = 5 Hz, 2 H_a). ¹³C NMR (DMSO-d₆) (Appendix 3) : δ 35.67 (C_e), 49.61 (C_r), 122.19 (C_c), 123.74 (C_b), 137.63

(C_d), 148.81 (C₂), 159.31 (C_g). **Analysis:** Calculate for C₁₄H₁₇Cl₂HgN₃: C, 33.71; H, 3.44; N, 8.42. Found : C, 33.68; H, 3.40; N, 8.33.

Synthesis of the Complex [Hg(TEPA)](ClO₄)₂. Solid Hg(ClO₄)₂ (0.9 g, 2.0 mmol) was dissolved in acetonitrile (2.0 mL) and added with stirring to a solution of TEPA (0.66 g, 2.0 mmol) in acetonitrile (2.0 mL). The resultant solution was filtered through celite into a 5 mm glass recrystallization tube and layered with ether. The solution was cooled to -40°C for 10 days and then allowed to warm to room temperature for 24 hours. Colorless, rectangular crystals grew which were not suitable for X-ray crystallography. The crystals were found to decompose between 150-160°C.

¹H NMR (CD₃CN) (Appendix 5) : δ 2.91 (m, 4 H_e), 3.03 (m, 4 H_f), 7.63 (d, J = 8 Hz, 2 H_d), 7.70 (t, J = 6 Hz, 2 H_b), 8.12 (t, J = 8 Hz, 2 H_c), 8.66 (d, J = 5 Hz, 2 H_a). ¹³C NMR (CNCD₃) (Appendix 5) : δ 36.49 (C_e), 56.32 (C_f), 126.38 (C_c, J = 26.9 Hz), 128.83 (C_b, J = 26.3 Hz), 143.84 (C_d), 152.14 (C_a), 163.18 (C_g). **Analysis:** Calculate for C₂₁H₂₄Cl₂HgN₄O₈ : C, 34.46; H, 3.31; N, 7.65. Found : C, 34.38; H, 3.32; N, 7.74.

X-ray Crystallography. Single crystal X-ray diffraction data were obtained in collaboration with Damon A. Parrish and Margaret E. Kastner at Bucknell University. Densities were measured by neutral buoyancy in bromoform/hexane solutions. Data were collected at room temperature on a Siemens R3 four-circle diffractometer using a graphite monochromated Mo K α X-radiation ($\lambda=0.71073\text{\AA}$) and the θ -2 θ technique over a range

of 3° to 55°. During data collection, three standard reflections were measured after every 50 reflections. Both crystals turned black in the beam. The structures were solved by direct methods and Fourier Difference Maps using the SHELXTL-PLUS³⁷ package of software programs. Final refinements were done using SHELXL-9322 minimizing $R2 = [\Sigma[w(F_o^2 - F_c^2)^2]] / \Sigma[w(F_o^2)^2]^{1/2}$, $R1 = \Sigma ||F_o| - |F_c|| / \Sigma |F_o|$, and $S = [\Sigma [w(F_o^2 - F_c^2)^2]] / (n - p)]^{1/2}$. All non-hydrogen atoms were refined as anisotropic and the hydrogen atomic positions were fixed relative to the bonded carbons and the isotropic thermal parameters were fixed.

NMR Measurements. All solutions for NMR analysis were prepared by adding stock solutions of BEPA or TEPA in acetonitrile-d₆ to a solution of mercuric perchlorate or mercuric chloride in acetonitrile-d₆ using calibrated autopipets. NMR spectra were recorded in 5-mm-o.d. NMR tubes on a General Electric QE-300 operating in the pulse Fourier transform mode. The sample temperature was maintained by blowing chilled air over the NMR tube in the probe. The variable temperature unit was calibrated with methanol as previously described.³⁸ Chemical shifts were measured and reported relative to internal solvents.

RESULTS AND DISCUSSION

I. ORGANIC SYNTHESIS

The ligands BEPA and TEPA were synthesized by the nucleophilic attack of an amine to an olefin as shown in Figure 2. Both ligands were susceptible to air oxidation and were therefore stored under argon at -20°C .

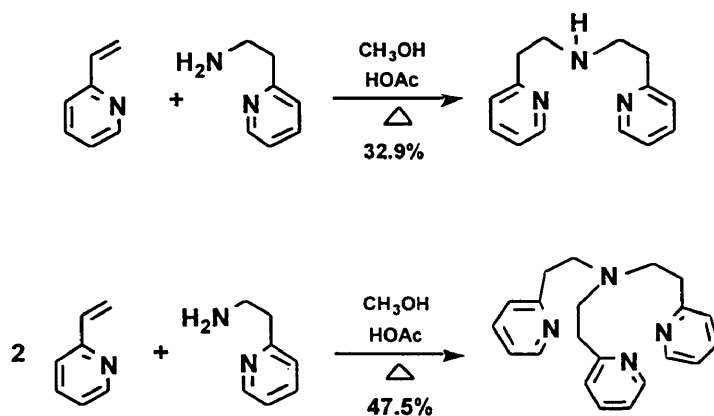


Figure 2. *Synthesis of BEPA and TEPA.*

BEPA was sufficiently volatile to permit isolation by vacuum distillation. One of the main problems associated with the synthesis of BEPA was separation from 2-vinylpyridine and 2-(2-aminoethyl)pyridine. Either decomposition of BEPA during distillation or volatilization of the 2-vinylpyridine and 2-(2-aminoethyl)pyridine fractions consistently led to trace contamination. The 2-vinylpyridine was readily removed from the final product under full vacuum (b.p. -2°C , 0.05 mm Hg) at room temperature. This technique was ineffective for removal of 2-(2-aminoethyl)pyridine from the desired product BEPA (b.p. 20°C , 0.05 mm Hg). Several attempts were made to eliminate 2-(2-aminoethyl)pyridine, utilizing such techniques as short path distillation, distillation using

a Claisen Vigreux distillation head and alumina chromatography. None of these methods proved effective as the contaminant was still detectable by GC-MS and NMR. Future optimization of the alumina chromatography solvent system may permit purification of the two components.

In order to form the tertiary amine TEPA, two equivalents of the olefin 2-vinylpyridine were used. The low volatility of TEPA prevented purification by vacuum distillation. Purification was effected by both flash chromatography using silica gel with 90% ethyl acetate/10% methanol saturated with ammonia and regular chromatography using alumina gel with 75% ethyl acetate/25% hexanes. The alumina column method was selected as the preferred method because it was less labor intensive and required less solvent than flash chromatography. Both methods gave comparable product yields.

II. X-RAY DIFFRACTION ANALYSIS STUDIES

CRYSTAL STRUCTURE OF [Hg(BEPA)](ClO₄)₂ (1). Crystals of this complex were grown from acetonitrile layered with toluene in 5 mm glass recrystallization tubes. Crystallographic data is shown in Table 1, the atomic coordinates are listed in Table 2, and selected bond lengths and bond angles are listed in Table 3 and Table 4, respectively. A thermal ellipsoid representation of [Hg(BEPA)](ClO₄)₂ is presented in Figure 3 .

[Hg(BEPA)](ClO₄)₂ crystallizes in the space group $P\bar{1}$ with $a = 10.950(3)$ Å, $b = 12.826(4)$ Å, $c = 13.035(4)$ Å, $\alpha = 67.39(2)^\circ$, $\beta = 82.74(2)^\circ$, and $\gamma = 68.09(2)^\circ$ with $Z = 2$. The asymmetric unit was found to contain a single cationic complex and two crystallographically unique perchlorates. There are significant bonding interactions to all

three ligand nitrogens with a Hg-N_{amine} distance of 2.510(8)Å and Hg-N_{pyridyl} distances of 2.104(6) Å and 2.114(6) Å. The N_{pyridyl}-Hg-N_{pyridyl} bond angle is 176.2°. Interestingly, the difference between the Hg-N_{amine} and Hg-N_{pyridyl} bond lengths is larger than in [Hg(BEPA)(Cl)₂], and their relative magnitudes are switched.

The perchlorate oxygen atoms are oriented towards the mercury ion to yield a distorted pseudo-octahedral environment. The cis bond angles range from 70.6° to 109.3° while the trans angles range from 154.0° to 176.2°. As seen in Figure 3, one perchlorate anion forms an asymmetric bridge.

CRYSTAL STRUCTURE OF [Hg(BEPA)Cl₂] (2). Crystals of this complex were grown from acetonitrile layered with 40% ethyl acetate/hexane in 5 mm glass recrystallization tubes. Crystallographic data is shown in Table 7, the atomic coordinates are listed in Table 8, and selected bond lengths and bond angles are listed in Table 9 and Table 10, respectively. A thermal ellipsoid representation of [Hg(BEPA)Cl₂] is presented in Figure 4 .

[Hg(BEPA)Cl₂] crystallizes in the orthorhombic space group Pnma with a = 13.424(3) Å, b = 14.854(3) Å, and c = 8.118(2) Å with Z = 4. The coordination sphere resembles that of [Hg(TLA)Cl₂],²⁵ in which one of the pyridyl groups of the potentially tetradentate ligand tris(6-methyl-2-pyridylmethyl)amine (TLA) is pendent. Similar to [Hg(TLA)Cl₂], the amine nitrogen and the two chlorides occupy the equatorial positions of a slightly distorted trigonal bipyramid while the pyridyl nitrogens occupy the axial positions. However, the [Hg(TLA)Cl₂] geometry is much closer to the ideal trigonal bipyramid shape since all the Hg-N bond lengths are comparable. This is an expected

consequence of the added flexibility of the six-membered chelate rings formed by BEPA versus the five membered chelate ring formed by TLA. The asymmetric unit of $[\text{Hg}(\text{BEPA})\text{Cl}_2]$ contains only half the molecule because the mercury atom, the two chlorides and the amine nitrogen lie on a mirror plane bisecting the 150° angle between the pyridine rings. The average $\text{N}_{\text{amine}}\text{-Hg-Cl}$ angle is 124.2° while the Cl-Hg-Cl angle is 111.7° . The pyridyl nitrogens are positioned slightly towards the $\text{Cl}(2)$ ion, creating one small $\text{Cl-Hg-N}_{\text{pyridyl}}$ angle (85.2°) and one larger angle (98.6°). The $\text{N}_{\text{amine}}\text{-Hg-N}_{\text{pyridyl}}$ bond angle is 86.0° and the $\text{N}_{\text{pyridyl}}\text{-Hg-N}_{\text{pyridyl}}$ bond angle is 162.5° .

In contrast to the similar $\text{Hg-N}_{\text{pyridyl}}$ and $\text{Hg-N}_{\text{amine}}$ bond lengths in the previously characterized HgCl_2 complexes of TLA and TMPA, the corresponding distances in $[\text{Hg}(\text{BEPA})\text{Cl}_2]$ vary considerably. The $[\text{Hg}(\text{BEPA})\text{Cl}_2]$ structure exhibits a $\text{Hg-N}_{\text{amine}}$ bond distance of 2.289 \AA , which is 0.260 \AA shorter than its $\text{Hg-N}_{\text{pyridyl}}$ bond distance of 2.549 \AA . The two Hg-Cl bond distances also differ in length. The $\text{Hg-Cl}(1)$ distance is 2.414 \AA while the $\text{Hg-Cl}(2)$ bond distance is 2.539 \AA . Steric crowding of $\text{Cl}(2)$ from the pyridyl nitrogens explains the observed discrepancy between the $\text{Hg-Cl}(1)$ and $\text{Hg-Cl}(2)$ bond distances.

DISCUSSION OF CRYSTAL STRUCTURES

Counterion selection has a significant impact on the structure of 1:1 complexes of Hg(II):BEPA . Chloride ions coordinate strongly to mercury, while perchlorate ions have only a slight tendency to serve as a ligand in complexes. Thus, perchlorates are widely used in studies of complex ion formation. The perchlorate ion can exercise monodendate,

bridging bidentate or chelating bidentate donor capacity if more strongly coordinating donors cannot complete the coordination sphere of a metal.²¹

The perchlorate ion has T_d symmetry and the characteristic Cl-O stretching mode occurs at about 1110 cm^{-1} , as a very broad band. A weak band is often found at about 980 cm^{-1} because of the infrared-forbidden totally symmetric stretching frequency. In compounds that contain unidentate perchlorates, there are three bands at about 1120 , 1040 , and 920 cm^{-1} , in accord with expectation for C_{3v} symmetry.²² A bidentate ClO_4^- exhibits stretching frequencies at about 1200cm^{-1} , 1100cm^{-1} , 1000cm^{-1} and 900cm^{-1} . The infra-red spectrum taken of $[\text{Hg}(\text{BEPA})](\text{ClO}_4)_2$ shows peaks at 1109cm^{-1} , 1045cm^{-1} and 927cm^{-1} . These data suggest that the perchlorates are unidentate and not bridging bidentate or chelating bidentate. In fact, the two shortest Hg-O bond distances measure 2.706\AA and 2.822\AA , much smaller than the combined van der Waal radii of mercury and oxygen (3.0\AA), further supporting the conclusion that the perchlorate ions are monodentate.²³ Close contact by a third monodentate perchlorate at 3.101\AA is long enough to be classified as non-bonding although oriented in a potentially bonding manner.

The BEPA ligand coordinates to Hg(II) through three nitrogen atoms, however the nature of this ligand forbids the trigonal planar arrangement seen in structures with three monodentate ligands.²⁴ The structure of $[\text{Hg}(\text{BEPA})](\text{ClO}_4)_2$ can be classified as pseudo-octahedral due to the presence of three perchlorate anions arranged near the Hg(II) ion. As seen in Figure 3, one perchlorate anion forms an asymmetric bridge. Interestingly, BEPA is able to bind equatorially forming a 1:1 complex, whereas the only other

structurally characterized Hg(II) complex of bis[(2-pyridyl)methyl]amine (BMPA) employs a capping geometry to form a 2:1 complex.²⁵

The Hg-N_{pyridyl} bonds are shorter than corresponding bond lengths measured in other three coordinate Hg (II) complexes containing Hg-N_{pyridyl} bonds.^{26,27,28,29} These complexes exhibit trigonal planar and T-shape geometry. Interestingly, the Hg-N_{pyridyl} bond distances measured in [Hg(BEPA)](ClO₄)₂ are more consistent with corresponding bond distances measured and reported for two coordinate mercury pyridine complexes.³⁰⁻
³⁶ Nevertheless, the structure of [Hg(BEPA)](ClO₄)₂ is undoubtedly three coordinate and the orientations of the perchlorates support classification as a five or six coordinate structure. The perchlorates arranged near the mercury yield a distorted octahedral environment.

For those compounds that are not regular octahedra, several kinds of distortion are possible. The first is tetragonal elongation, leaving four short bonds in a square planar arrangement together with two longer bonds above and below the plane. Second, is the reverse, a tetragonal compression with two short bonds on top and bottom and four longer bonds in the plane. The observed Hg-N_{pyridyl} bond length may be explained by the phenomena of tetragonal compression. The factors that could contribute to the compressed Hg-N_{pyridyl} bond observed in this complex are the formation of a less strained six-member chelate ring, the long Hg-N_{amine} bond distance of 2.510(8)Å and the linear relationship of the Hg-N_{pyridyl} bonds. In comparison, in [Hg(BMPA)₂](ClO₄)₂ the ligand is constrained to capping by five-member chelate rings and the Hg-N_{pyridyl} bond distance of the BMPA complex is lengthened by an average of 0.342Å.

In contrast to $[\text{Hg}(\text{BEPA})](\text{ClO}_4)_2$, the complex $[\text{Hg}(\text{BEPA})\text{Cl}_2]$ exhibits a distorted trigonal bipyramid geometry. The amine nitrogen and the two chlorides occupy the equatorial positions while the pyridyl nitrogens occupy the axial positions. The Hg- N_{amine} and Hg- $\text{N}_{\text{pyridyl}}$ bond distances of $[\text{Hg}(\text{BEPA})\text{Cl}_2]$ are 2.289Å and 2.549Å. Interestingly, the significant difference in the Hg- N_{amine} and Hg- $\text{N}_{\text{pyridyl}}$ bond distances of $[\text{Hg}(\text{BEPA})\text{Cl}_2]$ is unlike any other structures of HgCl_2 with nitrogen-based multidentate ligands reported so far. The complexes of $[\text{Hg}(\text{TMPA})\text{Cl}]_2(\text{HgCl}_4)$ and $[\text{Hg}(\text{TLA})\text{Cl}_2]$ exhibit similar Hg- N_{amine} and Hg- $\text{N}_{\text{pyridyl}}$ bond distances. The observed difference in the Hg- N_{amine} and Hg- $\text{N}_{\text{pyridyl}}$ bond distances of $[\text{Hg}(\text{BEPA})\text{Cl}_2]$ may be explained by a tetragonal elongation along the C_3 axis.

III. NMR SOLUTION STUDIES OF Hg(II) COORDINATION

The term “chemical exchange” encompasses both conformational changes and chemical reactions. The rate of exchange of metal-ligand complexes is a crucial factor in understanding the dynamics of the solution-state metal-exchange phenomenon. The fast exchange limit is approached when the exchange rate between two or more species is faster than the difference between the absorption frequencies of the two species. The fast exchange limit explains why spectral drifts are observed as the metal-to-ligand ratio is varied. The drifts are a result of a shift in equilibrium, as one complex becomes favored over the other.

The observation of heteronuclear coupling between the metal and ligand is also affected by the phenomenon of rapid exchange. The coupling constants of two species in equilibrium are averaged in a manner similar to chemical shifts. If one of those species is

in an uncoupled environment, typically no coupling is observed in the fast-exchange spectrum.

Intermediate exchange occurs when the equilibrium exchange rate is similar to the difference of the absorption frequencies of the two species.³⁹ Heteronuclear coupling is undetectable in these spectra due to residual line broadening of the proton resonances.

Slow exchange on the NMR time scale occurs when the exchange rate of the two species is slower than the difference in absorption frequencies.³⁹ Two distinct sets of resonances are observed for the two species. Heteronuclear coupling to the metal is observable with the relative intensity of the satellite peaks proportional to the natural abundance of the NMR active isotopes involved.

The ability to detect heteronuclear coupling is crucial to understanding the exchange dynamics and coordination chemistry of Hg(II) with BEPA and TEPA. Observations of satellites attributable to proton or carbon coupling to the ^{199}Hg nucleus have been rare due to the prevalence of rapid exchange of Hg(II) among ligating groups in solution at 20°C. Outside of the work conducted in this laboratory, we are aware of only one other synthetic complex of Hg(II) involving exclusively nitrogen donors for which $^3J(^1\text{H}^{199}\text{Hg})$ have been observed near 20°C.⁴⁰ The satellites were detected as small peaks symmetrical around a larger peak. The $^1\text{H}^{199}\text{Hg}$ satellites accounted for approximately 17% of the integrated area of the parent peak, as expected due to the 16.8% natural abundance of ^{199}Hg . Three-bond coupling constants as large as 30 Hz have been reported for the δ - or ϵ -protons of histidine in mercury substituted proteins.¹⁴ To examine the preferred coordination of BEPA and TEPA to Hg(II) in the solution-state, NMR analyses of $\text{Hg}(\text{ClO}_4)_2$ and HgCl_2 titrations with BEPA and TEPA were conducted. Interestingly,

heteronuclear coupling of hydrogen and carbon to mercury was observed at 20°C during several of these titrations.

Solution-State Investigations of BEPA Coordination of Hg(II). To investigate the solution structure and chemical exchange properties of BEPA complexes of Hg(II), solutions containing known molar ratios of ligand and either Hg(ClO₄)₂ or HgCl₂ in CD₃CN were examined by ¹H NMR. Solutions contained a total Hg(II) concentration of 2 mM. Additional studies were performed at 100 mM for purpose of comparison (data not shown). Summaries of proton chemical shifts during the separate titrations of Hg(ClO₄)₂ and HgCl₂ with BEPA are provided in Figure 5 and Figure 6. Selected proton spectra are shown in Figure 7 and Figure 8.

One distinct ligand environment with single ¹H chemical shifts for all symmetry related nuclei was observed for the pyridyl protons in the presence of 0.125 to 0.4375 equivalents of Hg(ClO₄)₂ at 20°C. The chemical shifts of all the proton resonances experienced a downfield drift (with the exception of H_a) as the equivalents of Hg(ClO₄)₂ were increased. Interestingly, the H_a proton shifted upfield initially with increased equivalents of Hg(ClO₄)₂, reaching a maximum upfield shift of 0.26 ppm at 0.5 equivalents. A shielding effect from the ring current of the opposite pyridyl ring would provide a plausible explanation for the upfield shift exhibited by the H_a proton. All other protons experienced downfield shifts which are an anticipated result of σ donation to a metal cation. The H_b, H_c, and H_d protons exhibited downfield shifts of 0.25, 0.27 and 0.24 ppm, respectively. The methylene protons, H_e and H_f, experienced the largest

change in chemical shift exhibiting downfield shifts of 0.28 and 0.48 ppm, respectively. All proton resonances were sharp and well resolved until the [Hg]/[BEPA] ratio equaled 0.5 and then peaks became severely exchanged broadened.

Above 0.5 equivalents of $\text{Hg}(\text{ClO}_4)_2$, the chemical shifts of all pyridyl protons changed rapidly until reaching a constant value at 0.875 equivalents. In the presence of 0.5 to 0.75 equivalents, no significant change in the chemical shift of the methylene protons was observed. However, above 0.75 equivalents the chemical shift changed rapidly until a complex methylene environment at 1.0 equivalent precluded further analysis. All proton resonances in the range of 0.5 to 0.9375 equivalents were severely exchanged broadened and no $^1\text{H}^{199}\text{Hg}$ couplings were observed until the $[\text{Hg}(\text{ClO}_4)_2]$ equaled the [BEPA]. At 1.0 equivalents of $\text{Hg}(\text{ClO}_4)_2$, all proton resonances became sharp, exhibiting $^3J(^1\text{H}^{199}\text{Hg})$ of 49 Hz to the H_a protons and $^4J(^1\text{H}^{199}\text{Hg})$ of 24 Hz to the H_d protons. The couplings reported here accounted for approximately 17% of the area of each resonance as expected based on the natural abundance of ^{199}Hg . The size and shape of the mercury satellites were unaffected by increasing amounts of $\text{Hg}(\text{ClO}_4)_2$ between 1.0 and 1.5 equivalents. The complex $[\text{Hg}(\text{BEPA})](\text{ClO}_4)_2$ has been isolated and structurally analyzed. This complex or possibly a solvate are proposed to account for the observed species at 1.0 equivalent of $\text{Hg}(\text{ClO}_4)_2$. The ^1H NMR spectra of crystals of $[\text{Hg}(\text{BEPA})](\text{ClO}_4)_2$ were identical to the equivalent samples prepared in situ.

One of the most notable features of these solution spectra was the change in the electronic environment surrounding the methylene protons at 1.0 equivalent of $\text{Hg}(\text{ClO}_4)_2$. At least four different methylene proton environments were observed

however, the complicated nature of this area of the spectrum precluded a detailed analysis and detection of coupling to Hg(II). It is suggested that a rapid exchange process which interconverts at least two species, for example, one with the central amine bound to Hg(II) and the other unbound, or perhaps conformational changes in the six-membered chelate ring might explain these observations. In order to further characterize the interconversion of this complex environment, acetonitrile solutions were cooled to -40°C . Considerable broadening of the methylene peaks at -40°C due to intermediate exchange rate processes prevented further analysis of the complex. In contrast, pyridyl resonances experienced minimal broadening upon cooling, consistent with preservation of the pyridyl N-Hg bonds during the process exchanging the methylene protons.

The spectra described above support the formation of cations with stoichiometry 1:2 and 1:1 of Hg(II) to BEPA in acetonitrile. The complex $[\text{Hg}(\text{BEPA})_2](\text{ClO}_4)_2$ is proposed to account for the 1:2 species. Although we have not yet been able to isolate this complex for structural analysis, we have prepared the related complex $[\text{Hg}(\text{BMPA})_2](\text{ClO}_4)_2$ where BMPA = bis-2-(2-pyridylmethyl)amine.⁴¹ A 1:1 complex of BEPA has been structurally characterized and is shown in Figure 3.

The chemical shifts of protons of BEPA were graphed as a function of the metal-to-ligand ratio, revealing a series of linked equilibria (Figure 5). Rapid exchange between free ligand and a 1:2 complex explains the approximately linear shift in all resonances between 0.125 and 0.5 equivalents of $\text{Hg}(\text{ClO}_4)_2$. Reactions (1) and (2) are consistent with the prevalent equilibrium at metal to ligand stoichiometries lower than 0.5.



Evidence for (1) was obtained from the graph of the chemical shifts of protons of BEPA as function of the metal-to-ligand ratio (Figure 5). A deviation above the ideal curve for the H_a proton provides evidence for the formation of at least two different complexes in this region of the titration. Similar equilibria have been suggested for a related tetradentate ligand, tris[(2-pyridyl)methyl]amine (TMPA).¹⁷

Possible structures for the 1:2 complex are shown in Figure 9. Rapid exchange between these conformations in solution would obscure detection of coupling to Hg(II).

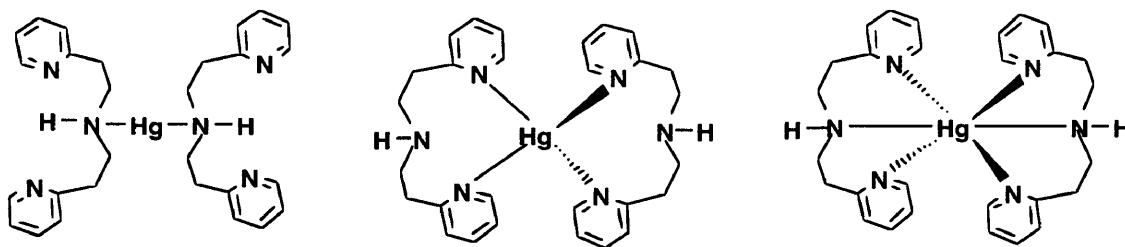
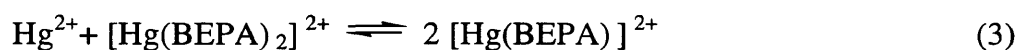


Figure 9. Proposed 1:2 complexes include BEPA binding as a monodentate, bidentate and tridentate ligand. Each of these complexes have additional geometric or structural isomers which are not shown.

In the presence of 0.5 to 0.75 equivalents of Hg(ClO₄)₂, all resonances become severely exchange broadened and chemical shifts of pyridyl resonances change rapidly with increasing equivalents of Hg(ClO₄)₂. Above 0.75 equivalents chemical shifts remain constant and resonances become well resolved at 1.0 equivalents of Hg(ClO₄)₂. The observation of a constant chemical shift above 0.75 equivalents of Hg(ClO₄)₂ may be

explained two ways. One explanation is that 0.75 is the stoichiometry of the terminal complex. This is unlikely because such a complex would be unsymmetrical and expected to exhibit a more complex NMR spectrum than what has been observed. Another possible explanation is an equilibrium between a 2:3 and 1:1 complex. The latter complexes must exhibit coincident chemical shifts to explain the observation of only one set of resonances. This explanation is conceivable if the bridging ligand and terminal ligands are in rapid exchange and the true coordination environment of the 1:1 complex is solvated by several CH₃CN molecules. This is also consistent with the absence of $J(^1\text{H}^{199}\text{Hg})$ until $[\text{Hg}]/[\text{BEPA}]$ is equal to or greater than one.

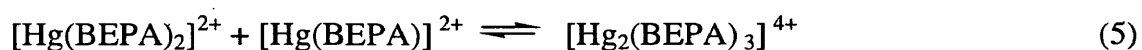
Further support of the existence of an multinuclear complex was obtained by graphing the chemical shifts of protons of BEPA as a function of the Hg(ClO₄)₂ to BEPA ratio. These plots strongly suggests involvement of another BEPA-containing species in the interconversion of the 1:2 and 1:1 species. For example, the formation of a 1:1 cation could occur directly from $[\text{Hg}(\text{BEPA})_2]^{2+}$ without formation of an intermediate 2:3 complex according to reaction (3):



Assuming that (i) the cations of $[\text{Hg}(\text{BEPA})_2]^{2+}$ and $[\text{Hg}(\text{BEPA})]^{2+}$ were the only BEPA-containing species in solution, and (ii) the changes in the chemical shift of each proton of the ligand molecule were primarily due to the formation of Hg-N bonds, the observed chemical shift δ_{obs} of the exchanged-averaged resonances should be given by the expression (4).

$$\delta_{\text{obs}} = P_{1:1}\delta_{1:1} + (1 - P_{1:1})\delta_{1:2} \quad (4)$$

The weighted average of the chemical shifts of the species present in solution is δ_{obs} . The chemical shifts of the two pure species in solution are given by $\delta_{1:1}$ and $\delta_{1:2}$ and their respective mole fractions within the equilibrium are represented by $P_{1:1}$ and $1 - P_{1:1}$.⁴² If the equilibrium of reaction (3) lies far to the right, then the solid line in Figure 5 represents the expected trend of the chemical shift. However, if the equilibrium of the reaction does not lie far towards product formation, a smooth curve which only approaches the line at a molar ratio greater than 1 is expected. Interestingly, in the presence of 0.5 to 0.75 equivalents of $\text{Hg}(\text{ClO}_4)_2$, a deviation above the ideal curve for the pyridyl protons was observed. This may be attributable to the existence of an intermediate complex of stoichiometry $\text{Hg}_2(\text{BEPA})_3$ with each $\text{Hg}(\text{II})$ coordinated to all three nitrogens of one BEPA and additional coordination by a BEPA bridging two metal ions. Reaction (5) and (6) illustrate the formation of the 3:2 and 1:1 complex.



Interestingly, a new ligand environment gradually appeared as equivalents of $\text{Hg}(\text{II})$ were increased from 1.0 to 1.5. These new resonances are possibly attributable to a 3:2 complex which becomes favored as additional equivalents of $\text{Hg}(\text{II})$ are added.

The coordination properties of BEPA with 100 mM $\text{Hg}(\text{ClO}_4)_2$ were studied for purpose of comparison. The chemical shifts of protons of BEPA graphed as a function of the $\text{Hg}(\text{ClO}_4)_2$ to BEPA ratio revealed a series of plots very similar to those observed at

Hg(II) concentrations of 2 mM. However, severely exchanged broadened resonances above 0.75 equivalents of $\text{Hg}(\text{ClO}_4)_2$ precluded detection of well resolved satellite peaks to the H_a and H_d protons. This is consistent with increased rates for associative ligand-exchange processes of ligand-Hg(II) complexes at high concentrations.

For comparison, the coordination properties of BEPA were also investigated with chloride counterions and total Hg(II) concentrations of 2 mM (Figures 6 and 8). Resonances associated with one ligand environment were observed for all equivalents of HgCl_2 with no heteronuclear coupling observable (Figure 8). In contrast to the perchlorate system, chemical shifts experienced a gradual, approximately linear change over all ratios of metal to ligand becoming essentially constant at or above 1.0 equivalents. Free ligand exchanged rapidly with the ligands of $[\text{Hg}(\text{BEPA})]^{2+}$ at 20°C at the concentrations examined. Select concentrations were cooled to -40°C in order to establish slow exchange conditions and further characterize the exchange processes. Rapid exchange prevailed at -40°C precluding detection of $J(^1\text{H}^{199}\text{Hg})$ coupling and further analysis.

In comparison to the perchlorate system, higher total Hg(II) concentrations were needed to form the 1:1 complex in the chloride system. This implies that the equilibrium constants for complex formation in this system are reduced. This may be attributed to the strong coordination of chloride ions to Hg(II), while perchlorate ions only have a slight tendency to serve as a ligand in Hg(II) complexes. Above 1:1, rapid exchange of ligands with excess Hg(II) could explain the inability to detect proton coupling to the ^{199}Hg nucleus.

Solution State Investigations of TEPA Coordination of Hg(II). To investigate the solution structure and chemical exchange properties of TEPA complexes of Hg(II), solutions containing known molar ratios of ligand and either Hg(ClO₄)₂ or HgCl₂ in CD₃CN were examined by ¹H NMR. All solutions contained a total Hg(II) concentration of 2 mM. Summaries of proton chemical shifts during the separate titrations of Hg(ClO₄)₂ and HgCl₂ are provided in Figures 10 and 11. Selected proton spectra are shown in Figures 12 and 13.

The occurrence of intermediate exchange in solution state Hg(II) coordination chemistry makes several features of these spectra very notable. One ligand environment, severely broadened due to intermediate exchange, was observed in the presence of 0.125 to 0.3125 equivalents of Hg(ClO₄)₂ (Figure 12). The chemical shifts of all protons remained approximately constant within this range, resembling free ligand. Above 0.3125 equivalents of Hg(ClO₄)₂, two exchange broadened ligand environments were observed. The new set of resonances appeared downfield from the first set and increased in intensity as more equivalents of Hg(II) were added. The first set of ligand resonances decreased in intensity with increased Hg(II) and disappeared completely at a [Hg]/[TEPA] slightly greater than 0.5. The new set of resonances exhibited ³J(¹H¹⁹⁹Hg) of 31 Hz to the H_a protons and ⁴J(¹H¹⁹⁹Hg) of 15 Hz to the H_d protons. The chemical shifts of these resonances remained constant up to a metal-to-ligand ratio of 1.5.

To further characterize the interconversion of these two complexes, selected solutions were cooled to -40°C. Severe broadening due to intermediate exchange conditions was apparent but two ligand environments were observed at metal-ligand ratios between 0.125 and 0.5. The chemical shifts for one set of ¹H resonances were very

similar to those for free ligand and the other set resembled the bound environment observed at 20°C. The set of peaks attributed to free ligand decreased in intensity as the equivalents of Hg(II) were increased. The second set of ^1H resonances increased in intensity as the equivalents of $\text{Hg}(\text{ClO}_4)_2$ were increased and exhibited $^3J(^1\text{H}^{199}\text{Hg})$ of 31 Hz to the H_a protons at 0.5 equivalents of $\text{Hg}(\text{ClO}_4)_2$. The chemical shifts of the apparent complex remained constant throughout the remainder of the titration.

The spectra described above support the formation of cations with stoichiometry 1:2 of Hg(II) to TEPA in acetonitrile. The complex $[\text{Hg}(\text{TEPA})_2](\text{ClO}_4)_2$ (Figure 14) is proposed to account for the 1:2 species although we have not yet been able to isolate this complex for structural analysis. A related eight-coordinate complex of TMPA has been characterized.¹⁷ This complex also exhibited slow exchange with free ligand in solution.

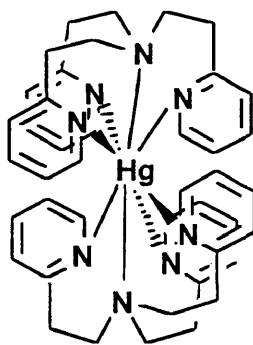
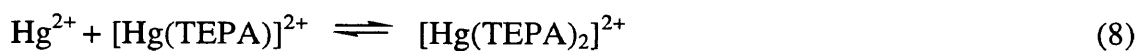


Figure 14. Proposed structure for $[\text{Hg}(\text{TEPA})_2](\text{ClO}_4)_2$.

The chemical shifts of the protons of TEPA were graphed as a function of the metal-to-ligand ratio revealing an equilibrium consistent with reaction (7) and (8).





Preliminary formation of a 1:1 metal-to-ligand complex with a lower formation constant is consistent with the small drifts in chemical shift for the “free ligand” environment. The most striking feature of the ^1H NMR spectra is existence of intermediate exchange between free ligand and the 1:2 complex. In contrast to the BEPA titration with Hg(II) where rapid exchange leads to exchanged averaged resonances, each TEPA resonance is seen as distinct in the ^1H NMR spectra. The consistency of chemical shift above $[\text{Hg}]/[\text{TEPA}] = 0.5$ suggests the formation constant for $[\text{Hg}(\text{TEPA})_2]^{2+}$ is considerably larger than the formation constant for $[\text{Hg}(\text{TEPA})]^{2+}$. Interestingly, a complex with stoichiometry $[\text{Hg}(\text{TEPA})]$ has been isolated which shows a solution-state spectrum very similar to the spectrum obtained at a $[\text{Hg}]/[\text{TEPA}] = 1.0$. X-ray diffraction analysis of this complex is needed before further conclusions can be drawn. Titrations with related ligand TMPA indicated that TMPA forms a 1:1 complex at high $[\text{Hg}]/[\text{TMPA}]$. TEPA does not appear to do this unless the chemical shifts of the 1:2 and 1:1 complexes are coincidentally identical.

Another interesting observation is the significant downfield shift from free ligand exhibited by the H_b , H_c , and H_d protons of the 1:2 complex of 0.56, 0.56 and 0.54 ppm, respectively. In contrast, the H_a , H_e and H_f exhibited much smaller downfield shifts of 0.18, 0.09 and 0.12, respectively. The small downfield shift of H_a and H_f is unusual. In work with related ligands, the protons closest to the Hg(II) typically experience the greatest change in chemical shift. A solid-state structure would facilitate explanation of this unique phenomenon.

For comparison, the coordination properties of TEPA were also investigated with chloride counterions and total Hg(II) concentrations of 2 mM (Figures 11, 13). Resonances associated with one ligand environment were observed for all equivalents of HgCl₂ with no heteronuclear coupling observable, presumably due to rapid exchange of the ligand between Hg(II) ions in solution. Similar to BEPA titrations with HgCl₂, chemical shifts experienced a gradual, approximately linear change over all ratios of metal to ligand. However, the magnitude of all equilibrium constants was clearly reduced. In the case of TEPA, constancy of proton chemical shifts required [Hg]/[TEPA] ≥ 2.0. Resonances were sharp and well resolved at all concentrations of [Hg]/[TEPA] due to rapid exchange at 20°C. Cooling to -40°C failed to establish slow exchange conditions although some broadening of resonances was apparent. Rapid exchange of free ligand with the ligands of [Hg(TEPA)]²⁺ is proposed as the equilibrium for this system. Titrations with related ligand TMPA and HgCl₂ indicated exchange between a 1:2 and 1:1 complex with the latter exhibiting ³J(¹H¹⁹⁹Hg) coupling of 45 and 24 Hz to the H_a and H_f protons, respectively.

CONCLUSION

The interpretation of the BEPA and TEPA NMR spectra has demonstrated some of the benefits of using ¹⁹⁹Hg in the characterization of processes involving ligand-metal exchange. We have demonstrated that heteronuclear coupling can provide detailed mechanistic and kinetic information about Hg(II)-coordination equilibria with potentially tridentate and tetradentate ligands. Cations of stoichiometry [Hg(BEPA)₂]²⁺ (**1**), [Hg(BEPA)]²⁺ and [Hg(BEPA)Cl₂] (**2**) were characterized by ¹H NMR in acetonitrile.

Protons of $[\text{Hg}(\text{BEPA})]^{2+}$ exhibited heteronuclear coupling to ^{199}Hg at 20°C as shown in the chart below. An additional complex with stoichiometry $[\text{Hg}_2(\text{BEPA})_3]^{4+}$ was proposed for the exchange of ligand between 1:2 and 1:1 metal to ligand complexes to explain deviations from the predicted chemical shift as a function of $[\text{Hg}]/[\text{BEPA}]$. In contrast, titrations with TEPA and $\text{Hg}(\text{ClO}_4)_2$ indicated that TEPA forms a 1:2 complex at high $[\text{Hg}]/[\text{TEPA}]$. Protons and carbons of these ligands exhibited heteronuclear coupling to ^{199}Hg at 20°C (shown below). Titrations of TEPA and BEPA with chloride counterions failed to exhibit heteronuclear coupling to ^{199}Hg , presumably due to rapid exchange of the ligand between $\text{Hg}(\text{II})$ ions in solution.

Compound	H_a (Hz)	H_d (Hz)	C_d	C_b
$[\text{Hg}(\text{BEPA})](\text{ClO}_4)_2$	49	24	N/A	N/A
$[\text{Hg}(\text{TEPA})_2](\text{ClO}_4)_2$	31	15	27	24

Significantly, the solution state NMR spectra were consistent with the solid state structures reported for the complexes (1) and (2). While correlations between solid state structures and solution state NMR properties must always be made cautiously,⁴³ compelling evidence for the formation of 1 and 2 in solution is provided by a combination of symmetry, shielding and heteronuclear coupling arguments. Mirror plane symmetry evident in the solid-state structures of both complexes was upheld in the solution-state. A cation believed to have a ligand geometry comparable to 1 in solution exhibited magnitudes of $^3J(^1\text{H}^{199}\text{Hg})$ and $^4J(^1\text{H}^{199}\text{Hg})$ consistent with significant bonding interactions between pyridyl nitrogens and $\text{Hg}(\text{II})$.

The relative ease of interpretation of these solution state spectra has motivated the investigation of the mercury coordination chemistry of additional multidentate ligands in our laboratory. Ligands with different chelate ring sizes and steric hindrance, as well as mixed donor ligands, are being examined (Figure 15). Ultimately, we hope to structurally characterize a wide variety of mercury-ligand complexes in order to add to the existing database of Hg(II) complexes and establish ^{199}Hg NMR as a unique spectroscopic probe. In the future, we hope to utilize the sensitivity of the tremendous chemical shift range of ^{199}Hg to draw comparisons between solution state ^{199}Hg chemical shifts of these and related complexes with their isotropic solid state chemical shifts.

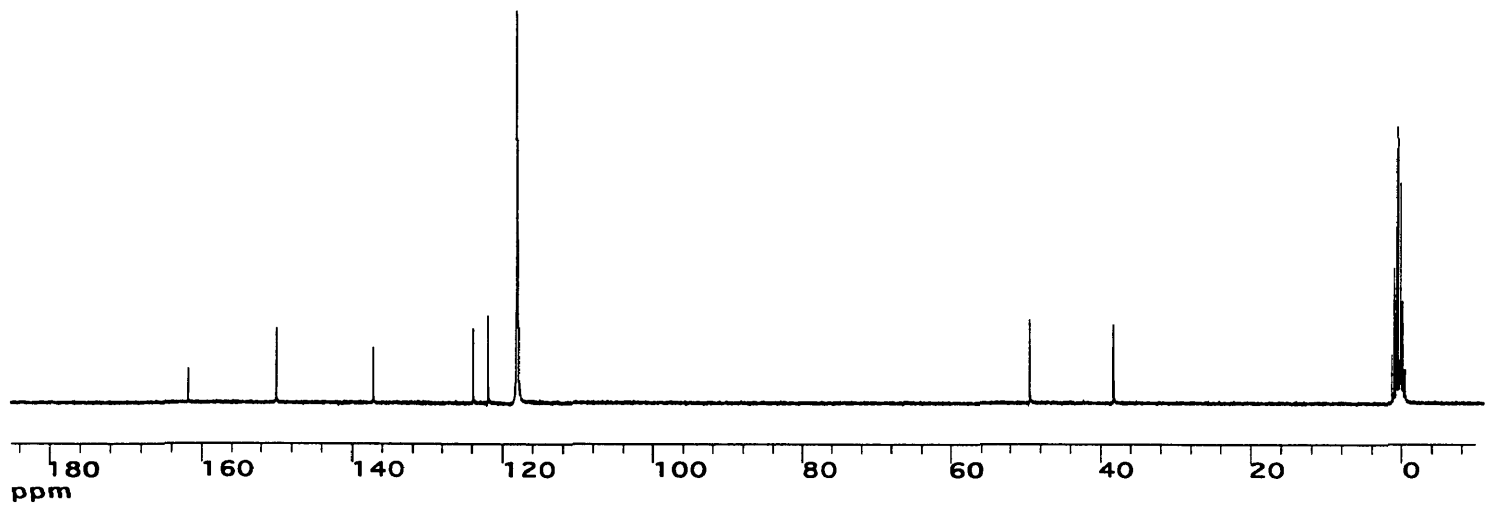
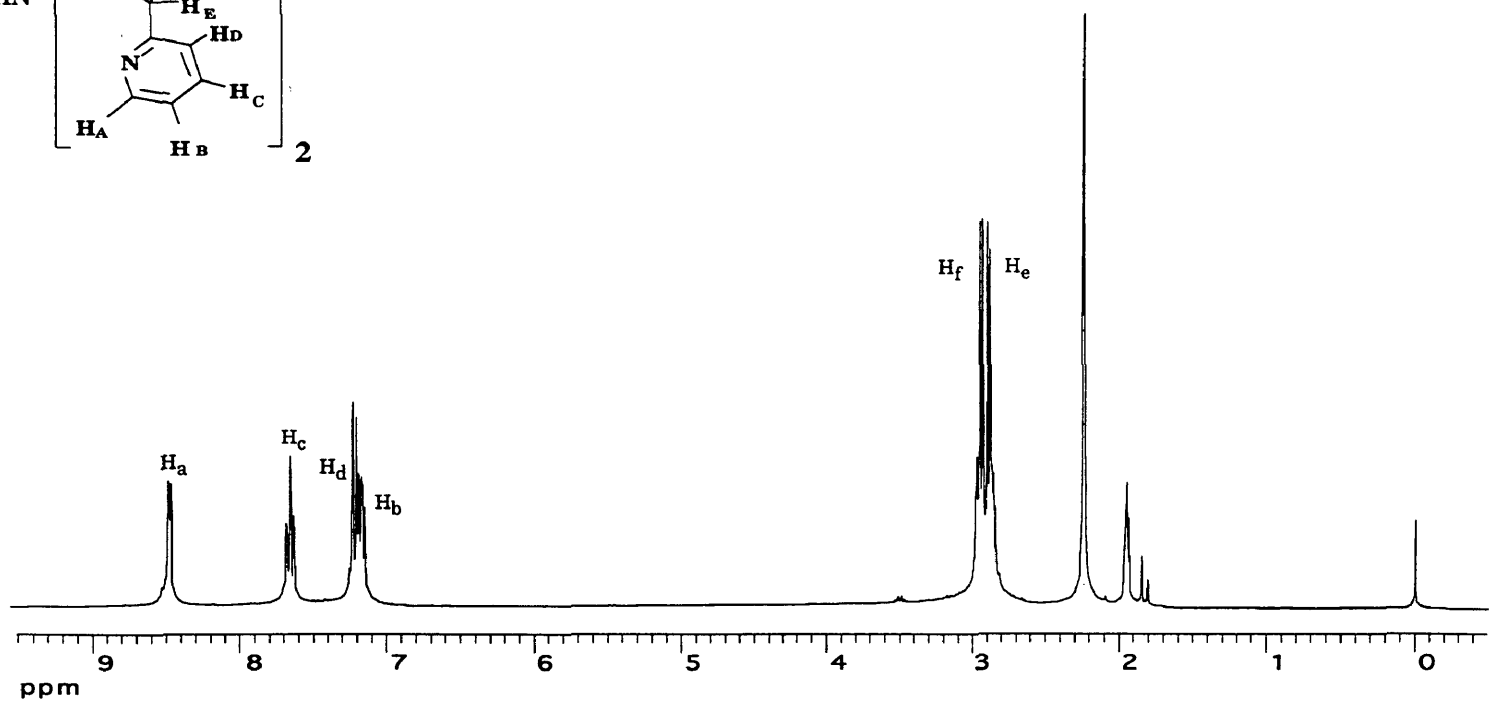
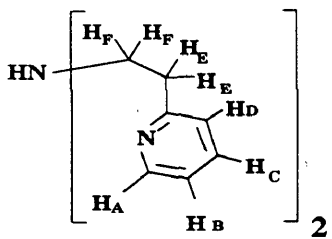
REFERENCES

- (1) *Biochemistry 2nd ed.*; Voet, D.; Voet, J.G., Ed.; John Wiley & Sons, INC.: New York, 1995, p 376.
- (2) Blake, P.R.; Lee, B.; Summers, M.F. *New J. Chem.* **1994**, *18*, 387-395.
- (3) Anfinsen, C.B.; Haber, E.; Sela, M.; White, F.H. *Proc. Natl. Acad. Sci. USA* **1961**, *47*, 1309-1314.
- (4) *Proteins, Structures and Molecular Properties, 2nd ed.*; Creighton, T.E., Ed.; W.H. Freeman & Co.: New York, 1993, p 309.
- (5) Balbach, J.; Forge, V.; van Nuland, N.A.J.; Winder, S.L.; Hore, P.J.; Dobson, C.M. *Nature, Struct. Biol.* **1995**, *2*, 865-870.
- (6) Bebout, D.C., grant proposal.
- (7) Hoeltzli, Sydney D.; Frieden, C. *Proc. Natl. Acad. Sci. USA* **1995**, *92*, 9318-9322.
- (8) Baldwin, R.L. *Curr. Opin. Struct. Biol.* **1993**, *3*, 84-91.
- (9) Englander, S.W.; Mayne, L. *Annu. Rev. Biophys. Biomol. Struct.* **1992**, *21*, 243-265.
- (10) (a) Hoeltzli, S.D.; Frieden, C. *Biochemistry* **1996**, *35*, 16843-16851. (b) Hoeltzli, S.D.; Frieden, C. *Proc. Natl. Acad. Sci. USA* **1995**, *92*, 9318-9322.
- (11) Cass, A.E.G.; Galdes *Dalton Trans.* **1994**, 1383. (b) McWhinnie, W.R.; Monsef-Mirzai, Z.; Perry, M.C.; Shaikh, N. *Polyhedron* **1993**, *12*, 1193.
- (12) Bebout, D.C. *J. Inorg. Chem.*, in press
- (13) (a) Wosley, W.C.J. *Chem. Ed.* **1973**, *50*, A355. (b) Raymond, K.N. *Chem. Eng. News* **1983**, *61* (49), 4.

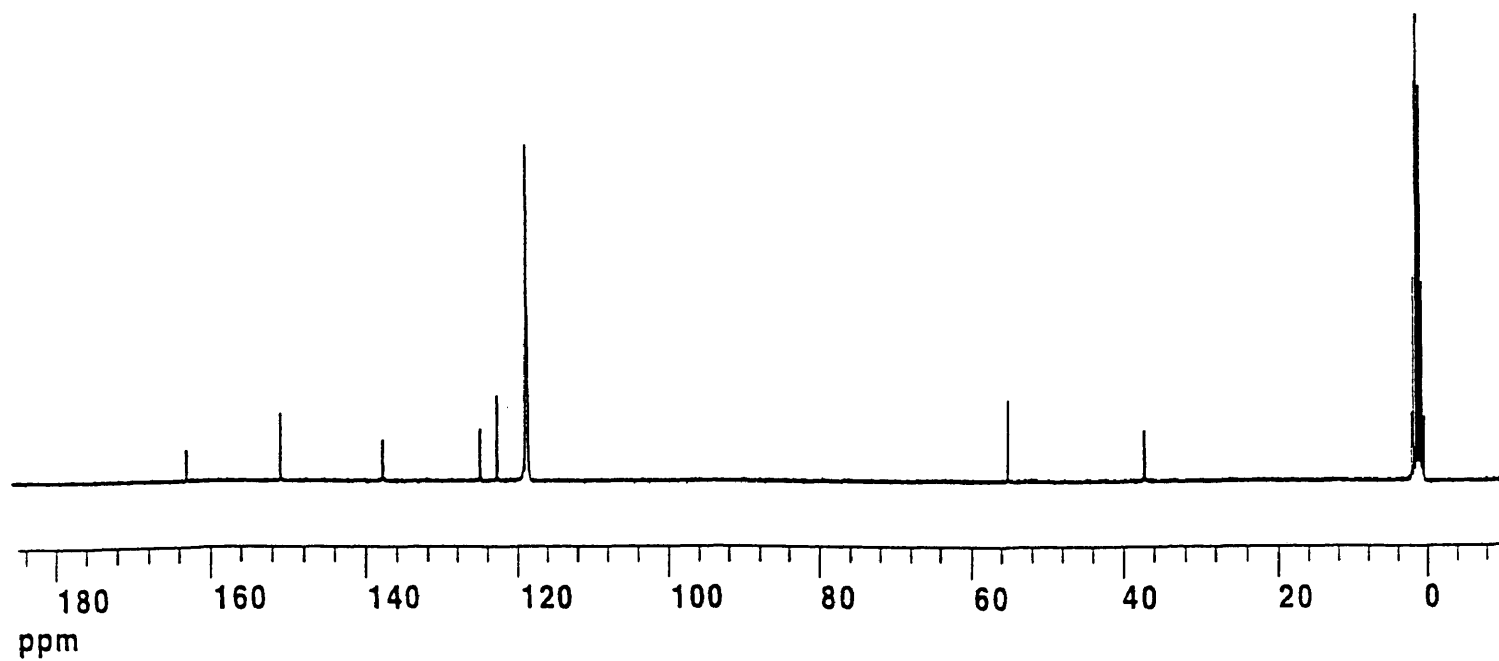
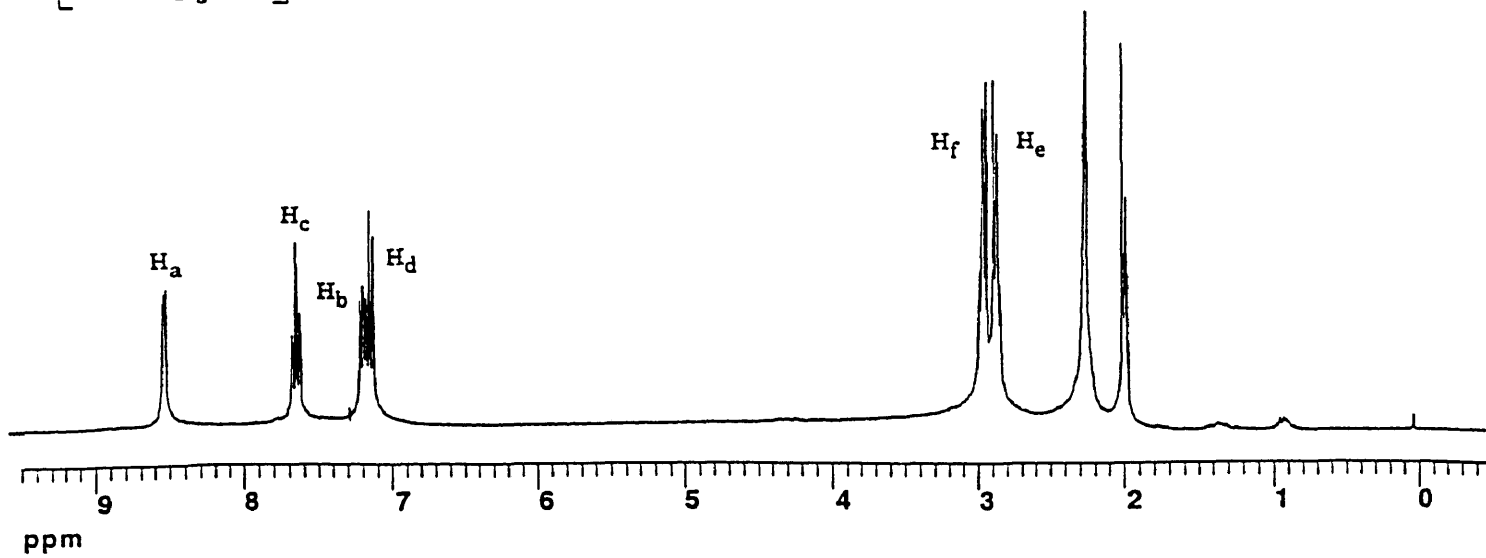
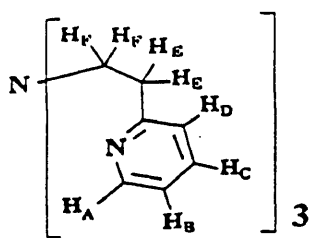
- (19) Romary, J.K.; Zachariassen, R.d.; Barger, J.D.; Schiesser, H.J. *J. Chem. Soc.* **1968**, *23*, 2884-2887.
- (20) Karlin, K.D.; Hayes, J.C.; Hutchinson, J.P.; Hyde, J.R., Zubieta *J. Inorg. Chim. Acta*, **1982**, *64*, L219-L220.
- (21) Christe, K.O.; Schack, C.J. *Inorg. Chem.*, **1974**, *13*, 1452.
- (22) *Advanced Inorganic Chemistry*, 4th ed., Cotton F.A., Wilkinson, G., Ed.; John Wiley & Sons, Inc.: New York, 1980, pp 174-175.
- (23) *Inorganic Chemistry: Principles of Structure and Reactivity* 4th ed., Huheey, J.E.; Keiter, E.A.; Keiter, R.L., Ed.; Harper Collins College Publishers: New York, 1993, p 291.
- (24) Halfpenny, J.; Small, R.W.H. *Acta. Cryst.*, **1978**, *B34*, 3758-3760.
- (25) DCB, KKC, MEK, DAP manuscript in preparation.
- (26) Halfpenny, J.; Small, R.W.H. *Acta. Cryst.*, **1978**, *B34*, 3758-3760.
- (27) Bochmann, M.; Webb, K.J.; Powell, A.K. *Polyhedron*, **1992**, *11*, 9513-9516.
- (28) Dieterich, S.; Strahle, J.Z. *Anorg. Allg. Chem.*, **1994**, *620*, 145-150.
- (29) Canty, A.J.; Chaichit, N.; Gatehouse, B.M.; George, E.E.; Hayhurst, G. *Inorg. Chem.*, **1981**, *20*, 2414-2422.
- (30) Halfpenny, J.; Small, R.W.H. *Acta. Cryst.*, **1981**, *B37*, 2223-2225.
- (31) Canty, A.J.; Chaichit, N.; Gatehouse, B.M. *Acta. Cryst.*, **1980**, *B36*, 786-789.
- (32) Baker, L.; Bowmaker, G.A.; Endrickson, N.J.; Skelton, B.W.; White, A.H. *J. Chem. Soc. Dalton Trans.*, **1992**, 2601-2606.
- (33) Canty, A.J.; Chaichit, N.; Gatehouse, B.M.; Marker, A. *Acta. Cryst.* **1978**, *B34*, 3229-3233.

- (34) Halfpenny, J.; Small, R.W.H.; Thorpe, F.G. *Acta. Cryst.*, **1978**, *B34*, 3075-3077.
- (35) Brownlee, R.T.C.; Canty, A.J.; Mackay, M.F. *Aust. J. Chem.*, **1978**, *31*, 1933-1936.
- (36) Kosturko, L.D.; Folzer, C.; and Stewart, R.F. *Biochemistry*, **1974**, *13*, 3949-3951.
- (37) SHELXTL-Plus, Version 4.21/V; Siemens Analytical X-ray Instr., Inc., **1990**.
- (38) Raiford, D.S.; Fisk, C.L.; Becker, E.D. *Anal. Chem.* **1979**, *51*, 2050.
- (39) *A Dictionary of Concepts on NMR*. Homans, S.W., Ed., Claridon Press; Oxford, **1989**, pp 31-34.
- (40) Schlager, O.; Wieghardt, K.; Grondey, H.; Ruffinska, A.; Nuber, B. *Inorg. Chem.* **1995**, *34*, 6440.
- (41) DCB, KKC, AED, DEE, MEK, DAP, RJB, manuscript in preparation.
- (42) Ghilardi, C.A., Midollini, S., Orlandini, A., and Vacca, A., *J. Chem. Soc., Dalton Trans.*, **1993**, *20*, 3117-3121.
- (43) Davies, J.A.; Dutremez, S. *Coord. Chem. Rev.* **1992**, *114*, 201.

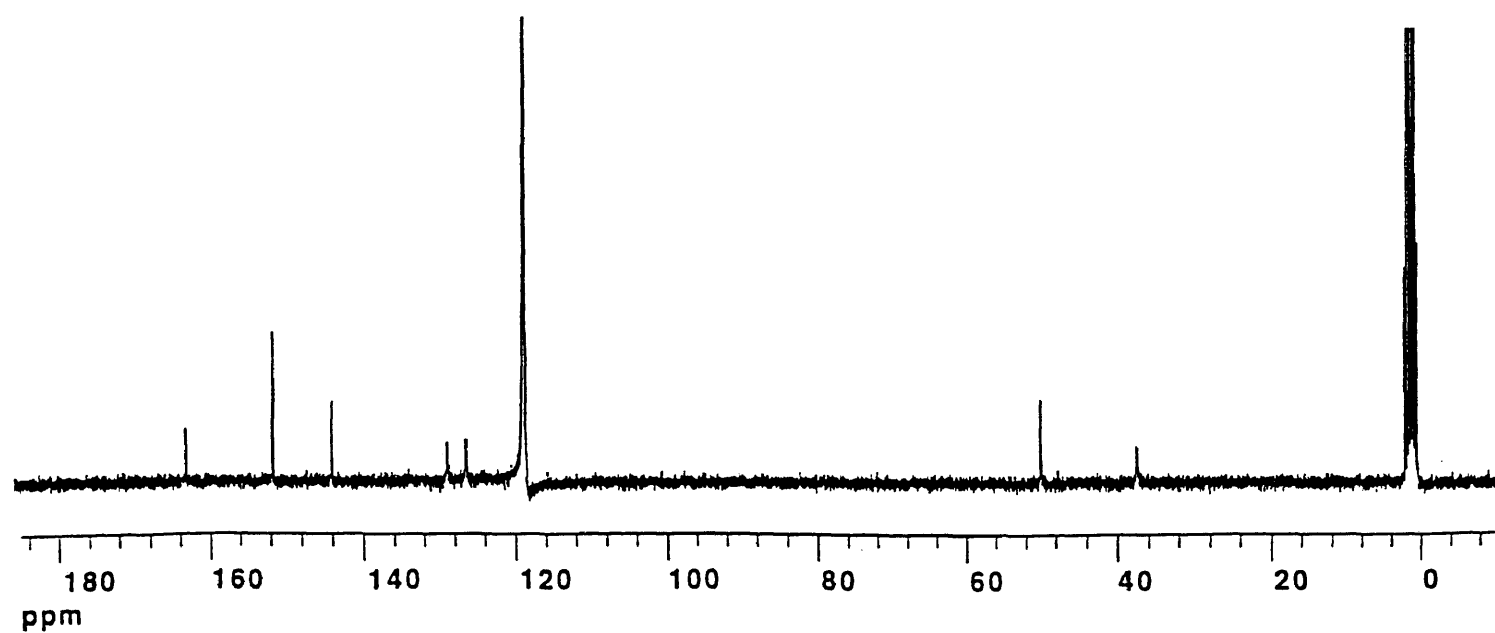
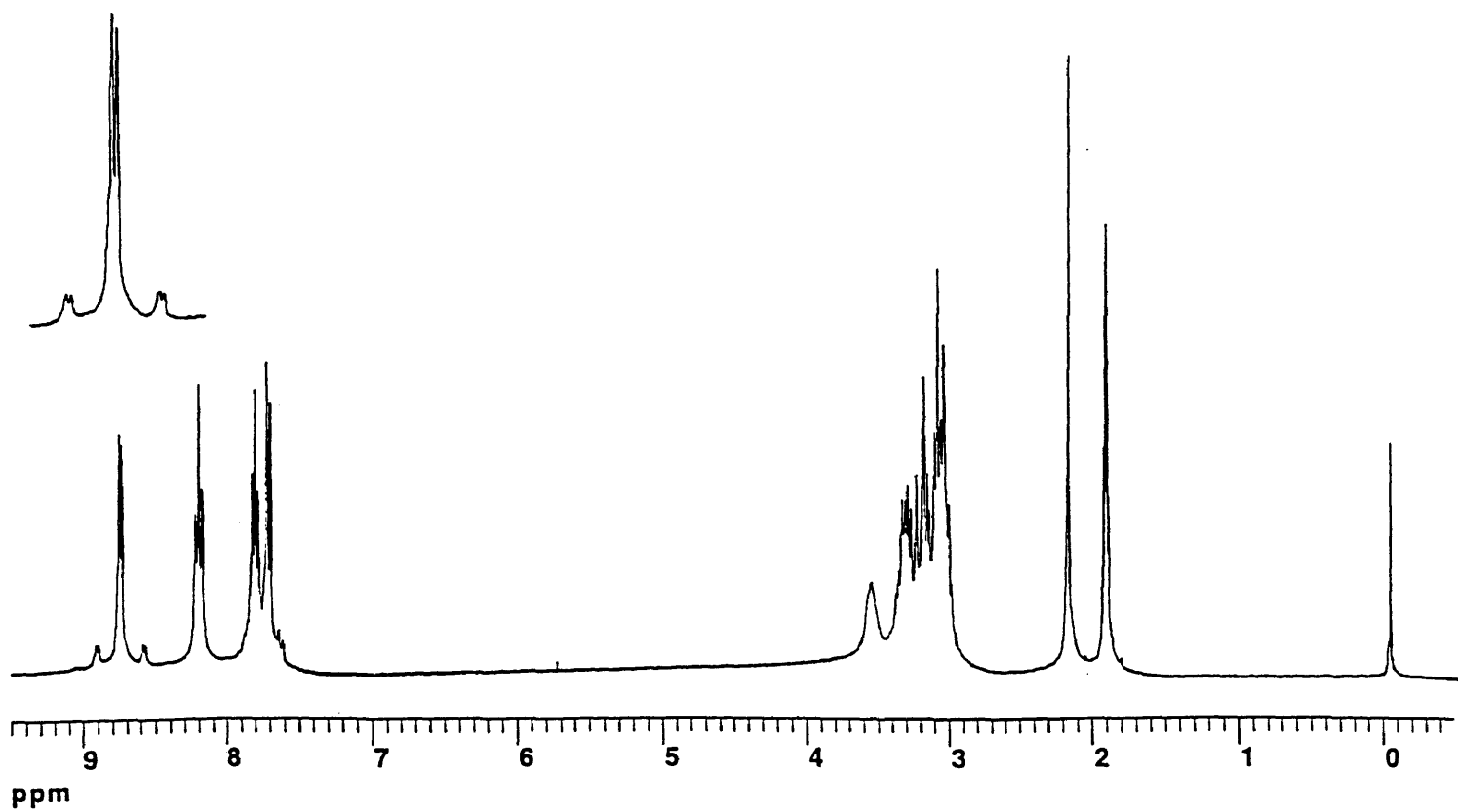
Appendix



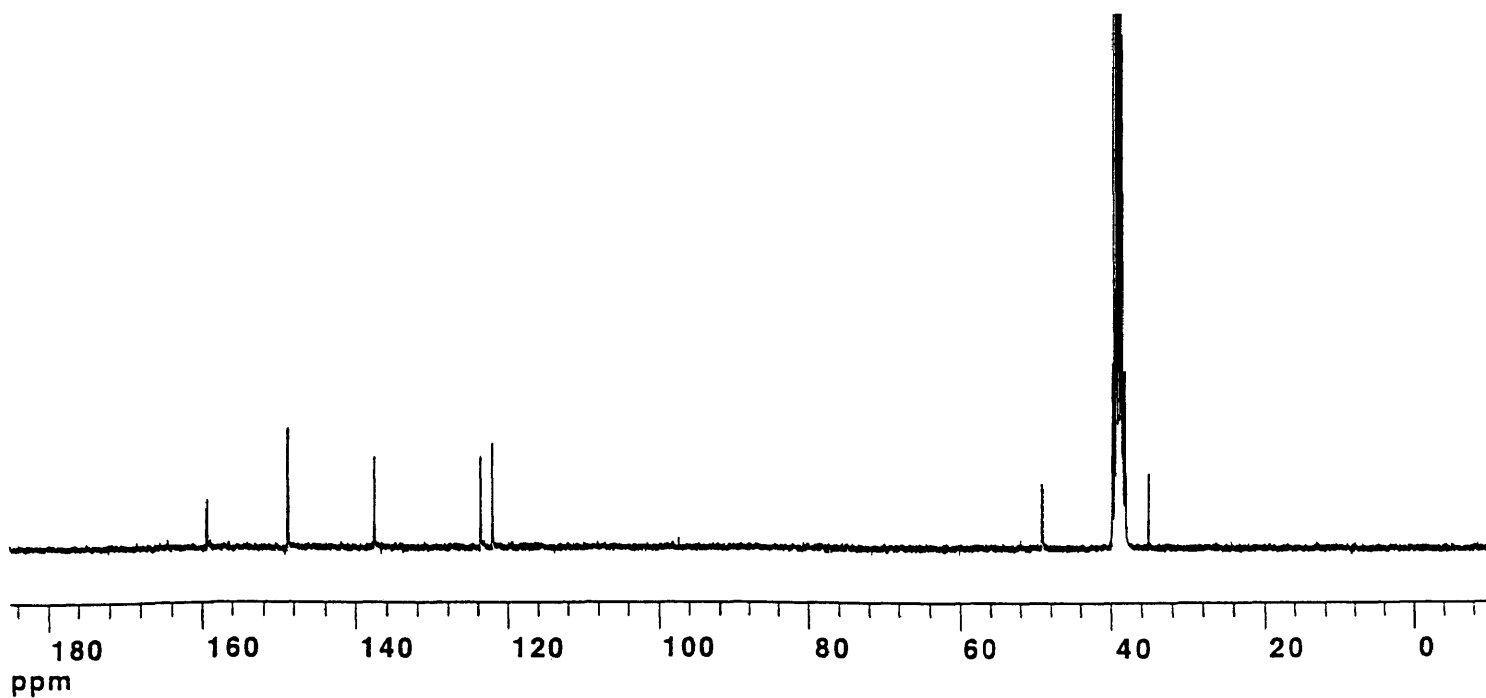
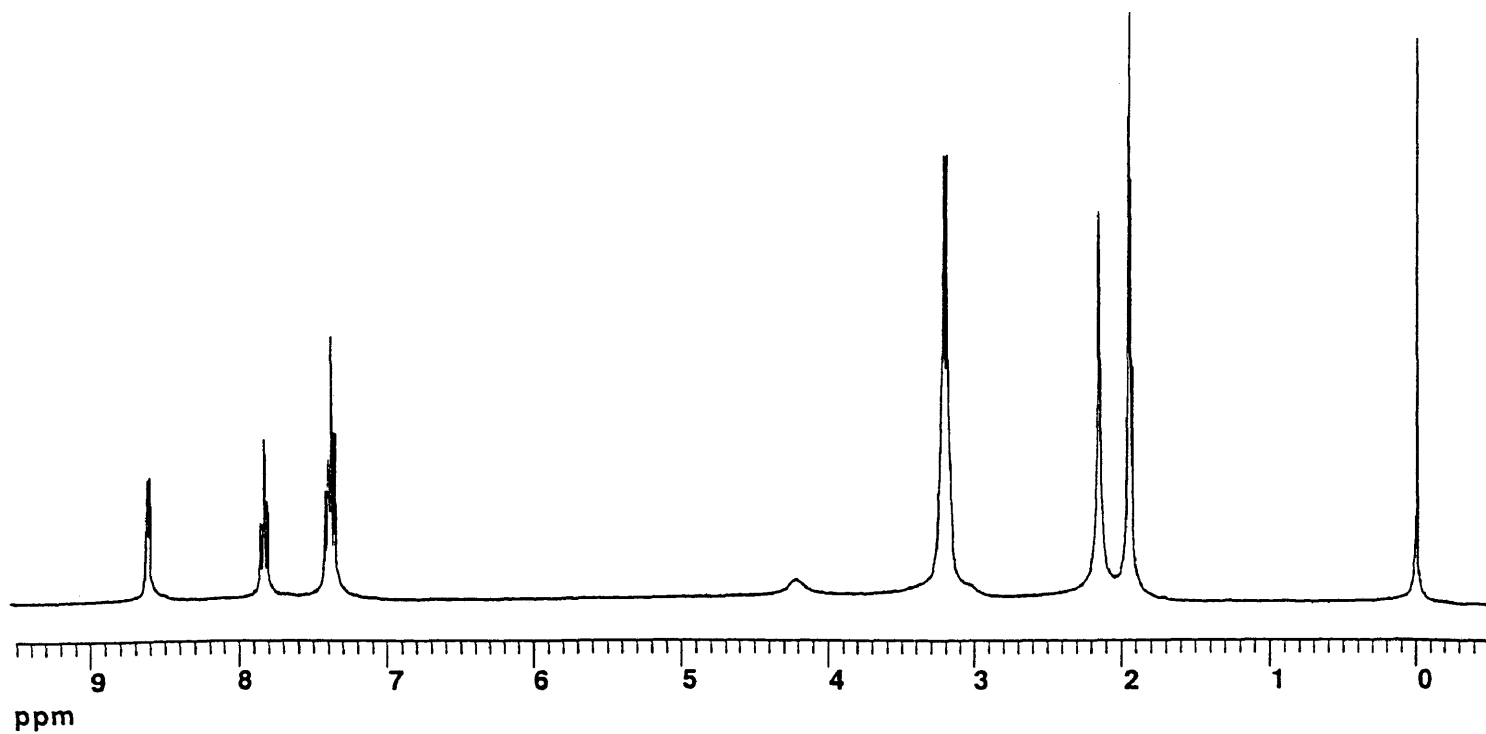
Appendix 1. ^1H NMR (top) and ^{13}C NMR (bottom) of BEPA.



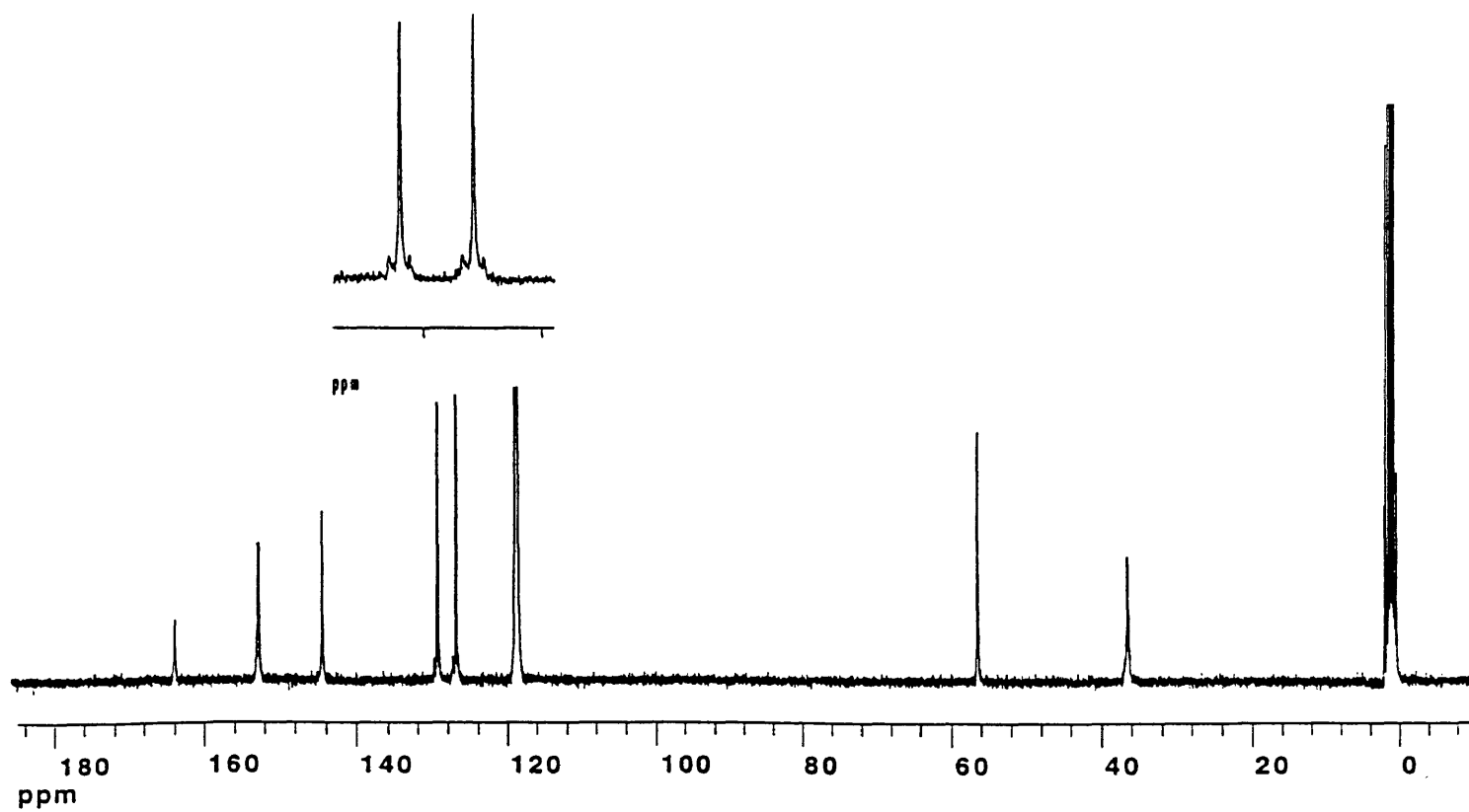
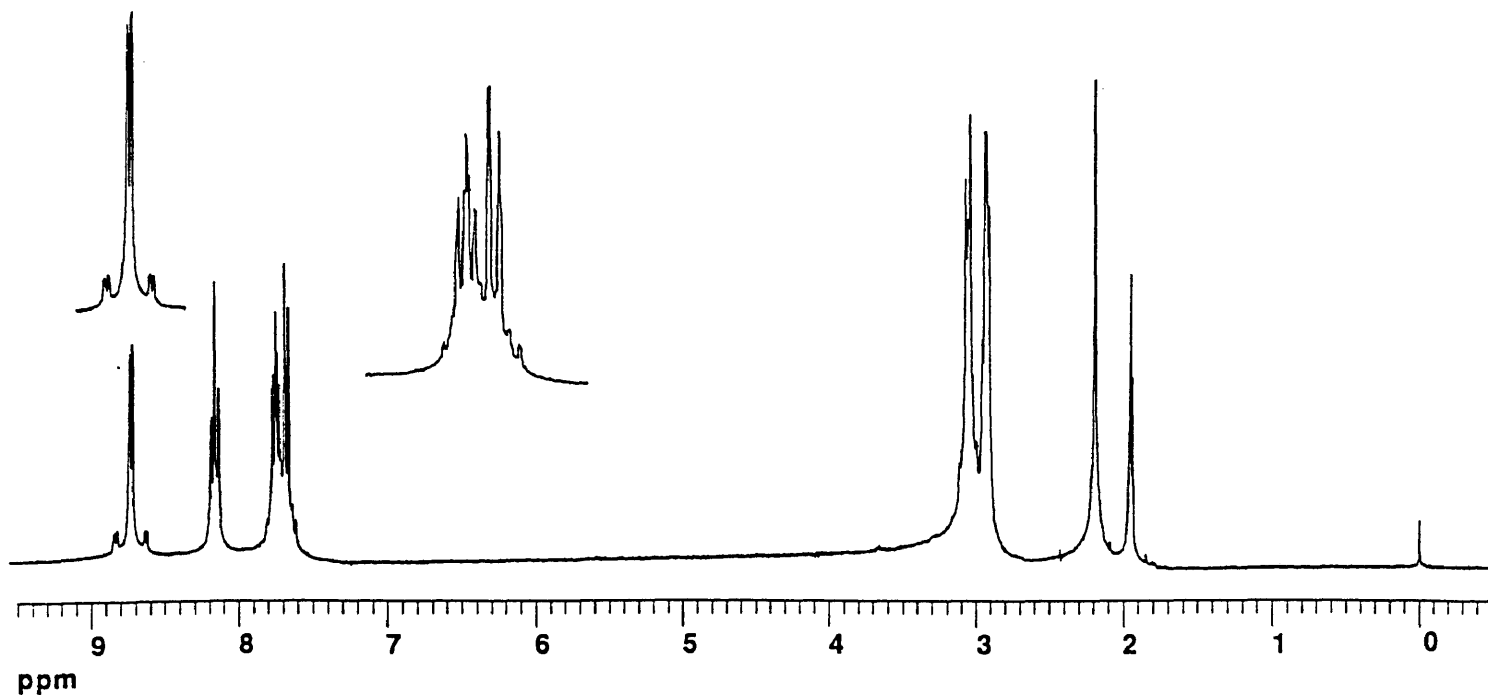
Appendix 2. ¹H NMR (top) and ¹³C NMR (bottom) of TEPA.



Appendix 3. ^1H NMR (top) and ^{13}C NMR (bottom) of $[\text{Hg}(\text{BEPA})](\text{ClO}_4)_2$.



Appendix 4. ^1H NMR (top) and ^{13}C NMR (bottom) of $[\text{Hg}(\text{BEPA})\text{Cl}_2]$.



Appendix 5. ^1H NMR (top) and ^{13}C NMR (bottom) of $[\text{Hg}(\text{TEPA})](\text{ClO}_4)_2$.

Table 1. Selected crystallographic data for [Hg(BEPA)](ClO₄)₂.

[Hg(BEPA)](ClO ₄) ₂	
formula	C ₁₄ H ₁₆ HgN ₃ Cl ₂ O ₈
formula weight	625.79
crystal dimensions (mm)	0.06 x 0.16 x 0.30
crystal color and habit	clear plate
crystal system	triclinic
space group	P $\bar{1}$
a (Å)	8.539(2)
b (Å)	9.160(3)
c (Å)	14.100(3)
α (°)	92.35(2)
β (°)	104.09(2)
γ (°)	117.31(2)
volume (Å ³)	935.4(4)
Z	2
D _{calc} (Mg m ⁻³)	2.222
D _{exp} (Mg m ⁻³)	2.23
μ (mm ⁻¹)	8.562
R [F ² > 2 σ (F ²)]	0.0367
wR (F ²)	0.1039
goodness of fit	0.765
number of standard reflections	3 / 50 reflections
limit along <i>h</i>	0 → 11
limit along <i>k</i>	-11 → 10
limit along <i>l</i>	-18 → 17
number reflections collected	4574
number independent reflections	4307
number observed reflections	3565
<i>I</i> > 2 σ (<i>I</i>)	
number parameters refined	253
data to parameter ratio	17:1
largest difference peak (e Å ⁻³)	1.572
largest difference hole (e Å ⁻³)	-1.450

Table 2. Atomic coordinates ($\times 10^4$) and equivalent isotropic displacement

parameters ($\text{\AA}^2 \times 10^3$) for $[\text{Hg}(\text{BEPA})](\text{ClO}_4)_2$. $U_{(\text{eq})}$ is defined as one third of the trace of the orthogonalized U_{ij} tensor.

Atom	x	y	z	$U_{(\text{eq})}$
Hg	2179(1)	2127(1)	2147(1)	36(1)
N	2148(9)	4291(8)	3282(4)	43(3)
N(1)	4138(8)	3944(8)	1575(4)	38(2)
N(2)	356(7)	332(7)	2805(4)	35(2)
C(1A)	5444(10)	3664(10)	1345(5)	43(3)
C(1B)	6881(11)	4886(11)	1104(5)	51(4)
C(1C)	7020(11)	6450(11)	1083(5)	51(3)
C(1D)	5683(12)	6697(10)	1319(6)	49(3)
C(1E)	4240(10)	5461(9)	1573(5)	40(3)
C(1F)	2837(13)	5795(11)	1856(6)	55(4)
C(1G)	3041(13)	5918(9)	2966(6)	53(4)
C(2A)	676(10)	-907(9)	3132(5)	41(3)
C(2B)	-276(11)	-1906(10)	3709(6)	50(4)
C(2C)	-1573(11)	-1634(10)	3974(6)	51(3)
C(2D)	-1906(10)	-376(10)	3647(6)	46(3)
C(2E)	-918(9)	625(9)	3061(5)	37(3)
C(2F)	-1202(10)	2025(10)	2702(5)	45(3)
C(2G)	245(12)	3758(10)	3322(7)	54(4)
Cl(1)	5775(2)	2804(2)	4252(1)	44(1)
O(1A)	6634(19)	4477(12)	4079(9)	144(7)
O(1B)	4425(12)	2713(16)	4663(6)	117(7)
O(1C)	7106(13)	2507(14)	4834(6)	109(6)
O(1D)	4962(8)	1754(9)	3296(4)	62(3)
Cl(2)	1839(2)	-1178(2)	191(1)	41(1)
O(2A)	3039(13)	-1722(13)	8(7)	104(6)
O(2B)	2267(14)	-611(11)	1210(5)	93(5)
O(2C)	72(14)	-2454(15)	-177(9)	162(7)
O(2D)	1852(18)	37(13)	-367(7)	123(8)

Table 3. Bond lengths (Å) for [Hg(BEPA)](ClO₄)₂.

Hg-N	2.510(8)	C(2A)-C(2B)	1.363(11)
Hg-N(1)	2.104(6)	C(2B)-C(2C)	1.369(16)
Hg-N(2)	2.114(6)	C(2C)-C(2D)	1.379(14)
N-C(1G)	1.475(10)	C(2D)-C(2E)	1.388(11)
N-C(2G)	1.484(13)	C(2E)-C(2F)	1.496(13)
N(1)-C(1A)	1.358(13)	C(2F)-C(2G)	1.540(9)
N(1)-C(1E)	1.353(11)	Cl(1)-O(1A)	1.426(10)
N(2)-C(2A)	1.358(11)	Cl(1)-O(1B)	1.383(12)
N(2)-C(2E)	1.355(12)	Cl(1)-O(1C)	1.374(12)
C(1A)-C(1B)	1.360(11)	Cl(1)-O(1D)	1.432(6)
C(1B)-C(1C)	1.385(15)	Cl(2)-O(2A)	1.397(14)
C(1C)-C(1D)	1.372(16)	Cl(2)-O(2B)	1.406(7)
C(1D)-C(1E)	1.376(11)	Cl(2)-O(2C)	1.365(9)
C(1E)-C(1F)	1.499(16)	Cl(2)-O(2D)	1.386(12)
C(1F)-C(1G)	1.526(12)		

Table 4. Bond angles (°) for [Hg(BEPA)](ClO₄)₂.

N-Hg-N(1)	92.6(2)	N(2)-C(2A)-C(2B)	121.8(9)
N-Hg-N(2)	86.7(2)	C(2A)-C(2B)-C(2C)	119.0(9)
N(1)-Hg-N(2)	176.2(2)	C(2B)-C(2C)-C(2D)	119.7(8)
Hg-N-C(1G)	108.7(5)	C(2C)-C(2D)-C(2E)	120.3(9)
Hg-N-C(2G)	110.4(4)	N(2)-C(2E)-C(2D)	119.0(8)
C(1G)-N-C(2G)	114.5(8)	N(2)-C(2E)-C(2F)	118.6(6)
Hg-N(1)-C(1A)	119.6(5)	C(2D)-C(2E)-C(2F)	122.4(8)
Hg-N(1)-C(1E)	119.3(6)	C(2E)-C(2F)-C(2G)	113.9(6)
C(1A)-N(1)-C(1E)	120.5(6)	N-C(2G)-C(2F)	114.0(8)
Hg-N(2)-C(2A)	120.4(5)	O(1A)-Cl(1)-O(1B)	104.3(9)
Hg-N(2)-C(2E)	118.2(5)	O(1A)-Cl(1)-O(1C)	108.6(7)
C(2A)-N(2)-C(2E)	120.2(6)	O(1B)-Cl(1)-O(1C)	116.0(6)
N(1)-C(1A)-C(1B)	121.5(9)	O(1A)-Cl(1)-O(1D)	106.2(6)
C(1A)-C(1B)-C(1C)	119.6(10)	O(1B)-Cl(1)-O(1D)	110.7(4)
C(1B)-C(1C)-C(1D)	117.6(7)	O(1C)-Cl(1)-O(1D)	110.5(6)
C(1C)-C(1D)-C(1E)	122.5(9)	O(2A)-Cl(2)-O(2B)	111.3(6)
N(1)-C(1E)-C(1D)	118.2(9)	O(2A)-Cl(2)-O(2C)	108.8(8)
N(1)-C(1E)-C(1F)	120.8(7)	O(2B)-Cl(2)-O(2C)	111.2(7)
C(1D)-C(1E)-C(1F)	120.9(8)	O(2A)-Cl(2)-O(2D)	110.2(8)
C(1E)-C(1F)-C(1G)	113.3(8)	O(2B)-Cl(2)-O(2D)	111.7(6)
N-C(1G)-C(1F)	114.1(6)	O(2C)-Cl(2)-O(2D)	103.3(8)

Table 5. Anisotropic displacement parameters ($\text{\AA}^2 \times 10^3$) for

$[\text{Hg}(\text{BEPA})](\text{ClO}_4)_2$. The anisotropic displacement factor exponent takes the

form: $-2\pi^2 [(\text{ha}^*)^2 U_{11} + \dots + 2\text{hka}^* \text{b}^* U_{12}]$

atom	U_{11}	U_{22}	U_{33}	U_{12}	U_{13}	U_{23}
Hg	36(1)	37(1)	43(1)	20(1)	19(1)	11(1)
N	43(3)	47(3)	40(3)	24(3)	14(3)	4(3)
N(1)	36(3)	45(3)	36(3)	20(3)	14(2)	11(2)
N(2)	31(3)	33(3)	44(3)	16(2)	16(2)	9(2)
C(1A)	41(4)	47(4)	39(3)	19(3)	14(3)	6(3)
C(1B)	40(4)	67(5)	41(4)	20(4)	17(3)	8(3)
C(1C)	44(4)	55(5)	38(4)	11(4)	13(3)	12(3)
C(1D)	62(5)	37(4)	40(4)	15(4)	18(3)	12(3)
C(1E)	43(4)	38(4)	37(3)	18(3)	13(3)	11(3)
C(1F)	75(6)	59(5)	56(4)	47(5)	30(4)	26(4)
C(1G)	71(5)	36(4)	59(5)	21(4)	39(4)	9(3)
C(2A)	38(4)	39(4)	47(4)	19(3)	13(3)	7(3)
C(2B)	52(4)	40(4)	58(5)	22(4)	15(4)	18(3)
C(2C)	48(4)	51(4)	48(4)	16(4)	22(3)	17(3)
C(2D)	40(4)	48(4)	48(4)	18(3)	18(3)	3(3)
C(2E)	31(3)	39(3)	35(3)	15(3)	8(3)	-2(3)
C(2F)	43(4)	59(5)	45(4)	32(4)	17(3)	13(3)
C(2G)	60(5)	44(4)	76(5)	31(4)	40(4)	11(4)
Cl(1)	39(1)	55(1)	39(1)	26(1)	10(1)	2(1)
O(1A)	170(11)	54(5)	157(10)	20(6)	35(8)	11(6)
O(1B)	92(6)	225(12)	67(5)	102(7)	30(4)	-4(6)
O(1C)	108(6)	191(10)	64(4)	122(7)	-11(4)	-13(5)
O(1D)	56(3)	86(5)	48(3)	41(3)	11(3)	-6(3)
Cl(2)	45(1)	43(1)	39(1)	24(1)	15(1)	5(1)
O(2A)	118(7)	154(9)	110(6)	110(7)	56(6)	37(6)
O(2B)	158(8)	94(6)	46(3)	84(6)	13(4)	-5(3)
O(2C)	86(7)	142(10)	152(10)	-33(7)	48(7)	-40(8)
O(2D)	237(13)	130(8)	95(6)	145(9)	79(7)	65(6)

Table 6. Hydrogen coordinates ($\times 10^4$) and isotropic displacement parameters ($\text{\AA}^2 \times 10^3$) for $[\text{Hg}(\text{BEPA})](\text{ClO}_4)_2$.

Atom	x	y	z	$U_{(\text{eq})}$
H(1AA)	5348	2579	1350	80
H(1BA)	7802	4666	958	80
H(1CA)	8018	7326	909	80
H(1DB)	5750	7771	1303	80
H(1FA)	1634	4888	1511	80
H(1FB)	2910	6799	1642	80
H(1GA)	4335	6467	3315	80
H(1GB)	2544	6600	3149	80
H(2AA)	1600	-1085	2956	80
H(2BB)	-54	-2795	3918	80
H(2CA)	-2228	-2300	4398	80
H(2DA)	-2843	-204	3810	80
H(2FA)	-2407	1829	2702	80
H(2FB)	-1156	2027	2028	80
H(2GA)	-104	4573	3100	80
H(2GB)	244	3733	4002	80

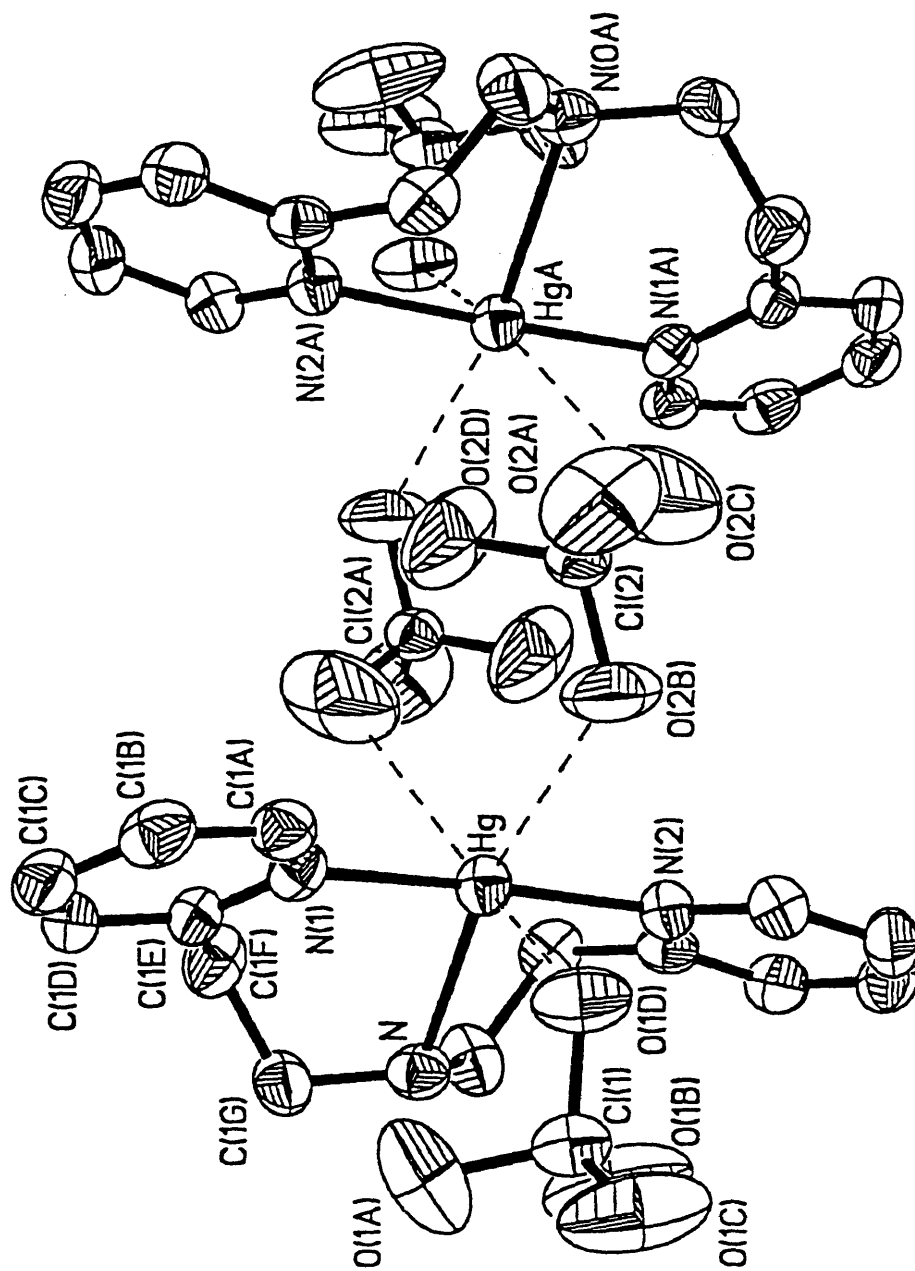


Figure 3. Thermal ellipsoid plot of the pseudo-octahedral arrangement of the dimer association of $[\text{Hg}(\text{BEPA})](\text{ClO}_4)_2$. Ellipsoids represent 50% probability electron density of the atom.

Table 7. Selected crystallographic data for [Hg(BEPA)Cl₂].

[Hg(BEPA)Cl ₂]	
formula	C ₁₄ H ₁₆ HgCl ₂ N ₃
formula weight	497.8
crystal dimensions (mm)	0.16 x 0.23 x 0.40
crystal color and habit	clear colorless prism
crystal system	orthorhombic
space group	Pnma
a (Å)	13.424(3)
b (Å)	14.854(3)
c (Å)	8.118(2)
α (°)	90.0
β (°)	90.0
γ (°)	90.0
volume (Å ³)	1618.7(6)
Z	4
D _{calc} (Mg m ⁻³)	2.043
D _{exp} (Mg m ⁻³)	
μ (mm ⁻¹)	9.832
R [F ² > 2σ(F ²)]	0.0452
wR (F ²)	0.1145
goodness of fit, S	0.928
number of standard reflections	3/50
limit along <i>h</i>	0→17
limit along <i>k</i>	0→19
limit along <i>l</i>	0→10
number reflections collected	1942
number independent reflections	1942
number observed reflections	1484
<i>I</i> > 2σ(<i>I</i>)	
number parameters refined	97
data to parameter ratio	20:1
largest difference peak (e Å ⁻³)	2.259
largest difference hole (e Å ⁻³)	-0.942

Table 8. Atomic coordinates ($\times 10^4$) and equivalent isotropic displacement parameters ($\text{\AA}^2 \times 10^3$) for $[\text{Hg}(\text{BEPA})\text{Cl}_2]$. $U_{(\text{eq})}$ is defined as one third of the trace of the orthogonalized U_{ij} tensor.

Atom	x	y	z	$U_{(\text{eq})}$
Hg	3841(1)	2500	2264(1)	44(1)
Cl(1)	3667(3)	2500	-696(7)	81(3)
Cl(2)	5657(3)	2500	3137(6)	59(2)
N(1)	2614(8)	2500	4224(15)	41(5)
N(2)	3924(12)	4196(11)	2721(16)	58(6)
C(1A)	4723(13)	4631(15)	2148(15)	69(8)
C(1B)	4929(11)	5497(15)	2439(17)	71(8)
C(1C)	4299(16)	5964(10)	3456(22)	83(7)
C(1D)	3492(11)	5542(11)	4068(15)	60(7)
C(1E)	3324(11)	4665(10)	3675(18)	45(5)
C(1F)	2406(9)	4163(9)	4303(17)	72(6)
C(1G)	2627(8)	3315(7)	5260(15)	64(6)

Table 9. Bond lengths (\AA) for $[\text{Hg}(\text{BEPA})\text{Cl}_2]$.

Hg-Cl(1)	2.414(5)	N(2)-C(1E)	1.317(21)
Hg-Cl(2)	2.539(4)	C(1A)-C(1B)	1.338(31)
Hg-N(1)	2.289(11)	C(1B)-C(1C)	1.371(25)
Hg-N(2)	2.549(16)	C(1C)-C(1D)	1.347(25)
Hg-N(2A)	2.549(16)	C(1D)-C(1E)	1.361(21)
N(1)-C(1G)	1.474(13)	C(1E)-C(1F)	1.527(20)
N(1)-C(1GA)	1.474(13)	C(1F)-C(1G)	1.509(17)
N(2)-C(1A)	1.335(24)		

Table 10. Bond angles (°) for [Hg(BEPA)Cl₂].

Cl(1)-Hg-Cl(2)	111.7(2)	Hg-N(2)-C(1A)	117.6(13)
Cl(1)-Hg-N(1)	128.5(3)	Hg-N(2)-C(1E)	125.5(11)
Cl(2)-Hg-N(1)	119.8(3)	C(1A)-N(2)-C(1E)	116.2(16)
Cl(1)-Hg-N(2)	98.6(3)	N(2)-C(1A)-C(1B)	124.8(16)
Cl(2)-Hg-N(2)	85.2(4)	C(1A)-C(1B)-C(1C)	117.7(15)
N(1)-Hg-N(2)	86.0(3)	C(1B)-C(1C)-C(1D)	118.9(15)
Cl(1)-Hg-N(2A)	98.6(3)	C(1C)-C(1D)-C(1E)	119.6(14)
Cl(2)-Hg-N(2A)	85.2(4)	N(2)-C(1E)-C(1D)	122.8(14)
N(1)-Hg-N(2A)	86.0(3)	N(2)-C(1E)-C(1F)	115.6(13)
N(2)-Hg-N(2A)	162.5(6)	C(1D)-C(1E)-C(1F)	121.6(13)
Hg-N(1)-C(1G)	112.8(6)	C(1E)-C(1F)-C(1G)	114.9(11)
Hg-N(1)-C(1GA)	112.8(6)	N(1)-C(1G)-C(1F)	112.9(10)
C(1G)-N(1)-C(1GA)	110.4(12)		

Table 11. Anisotropic displacement parameters ($\text{\AA}^2 \times 10^3$) for [Hg(BEPA)Cl₂].

The anisotropic displacement factor exponent takes the form:

atom	U ₁₁	U ₂₂	U ₃₃	U ₁₂	U ₁₃	U ₂₃
Hg	48(1)	43(1)	42(1)	0	7(1)	0
Cl(1)	130(5)	63(4)	51(4)	0	-8(3)	0
Cl(2)	44(3)	56(3)	77(4)	0	-6(3)	0
N(1)	40(9)	47(9)	35(10)	0	12(6)	0
N(2)	67(11)	42(11)	64(10)	18(9)	-3(7)	-21(8)
C(1A)	37(12)	74(17)	98(13)	-3(9)	20(8)	23(11)
C(1B)	66(13)	48(12)	99(16)	-34(11)	-26(10)	18(9)
C(1C)	117(15)	47(10)	84(13)	6(13)	-34(11)	-19(10)
C(1D)	81(12)	51(13)	49(10)	3(9)	2(9)	-9(8)
C(1E)	65(10)	26(9)	44(9)	-7(10)	-4(8)	-3(8)
C(1F)	84(12)	68(10)	65(12)	28(9)	6(8)	-28(9)
C(1G)	82(10)	55(10)	54(10)	6(7)	25(7)	2(8)

Table 12. Hydrogen coordinates ($\times 10^4$) and isotropic displacement parameters ($\text{\AA}^2 \times 10^3$) for $[\text{Hg}(\text{BEPA})\text{Cl}_2]$.

Atom	x	y	z	$U_{(eq)}$
H(1AA)	5151	4299	1421	80
H(1BA)	5508	5781	1975	80
H(1CA)	4440	6577	3754	80
H(1DA)	3029	5866	4746	80
H(1FA)	1998	4555	4957	80
H(1FB)	2022	3976	3366	80
H(1GA)	2163	3240	6150	80
H(1GB)	3280	3392	5719	80

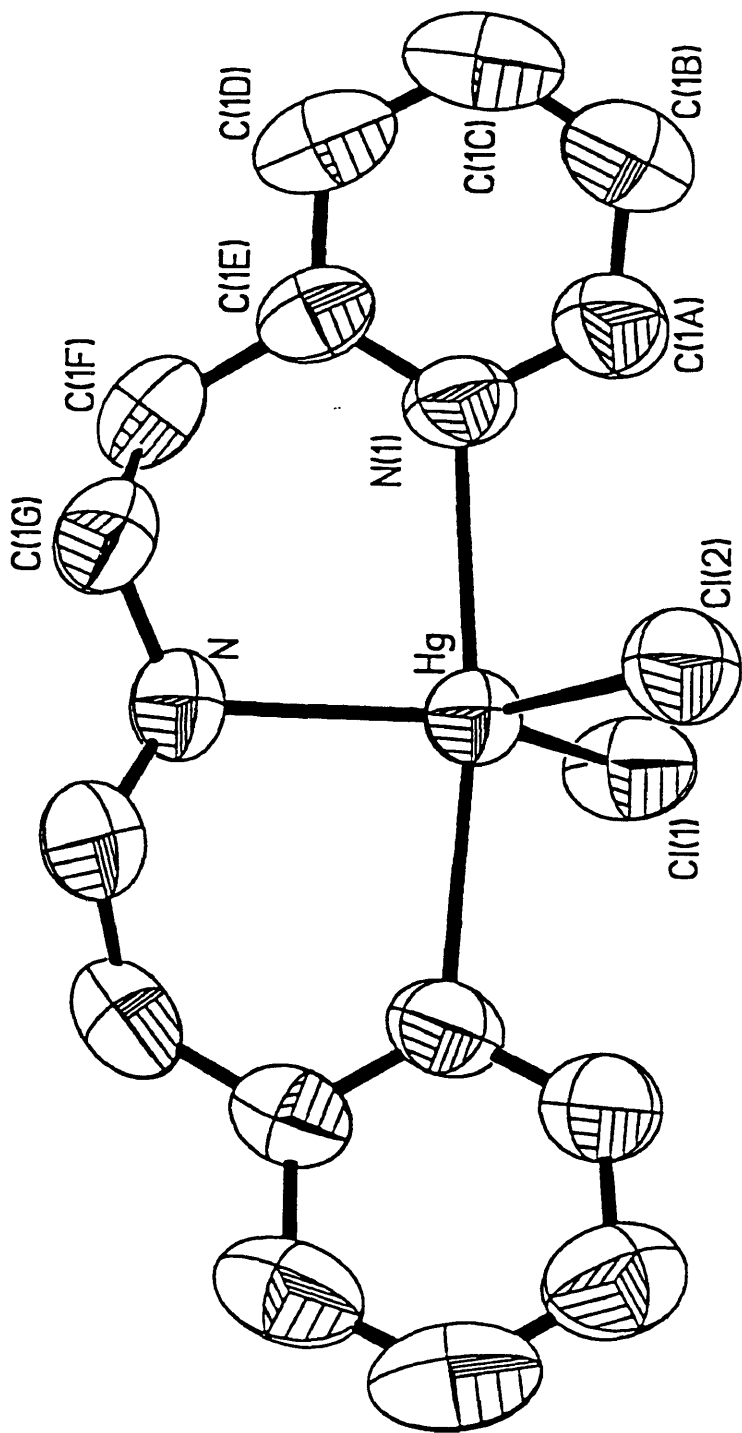


Figure 4. Thermal ellipsoid plot of [Hg(BEPA)Cl₂]. Ellipsoids represent 50% probability electron density of the atom. Hydrogen atoms are omitted for clarity.

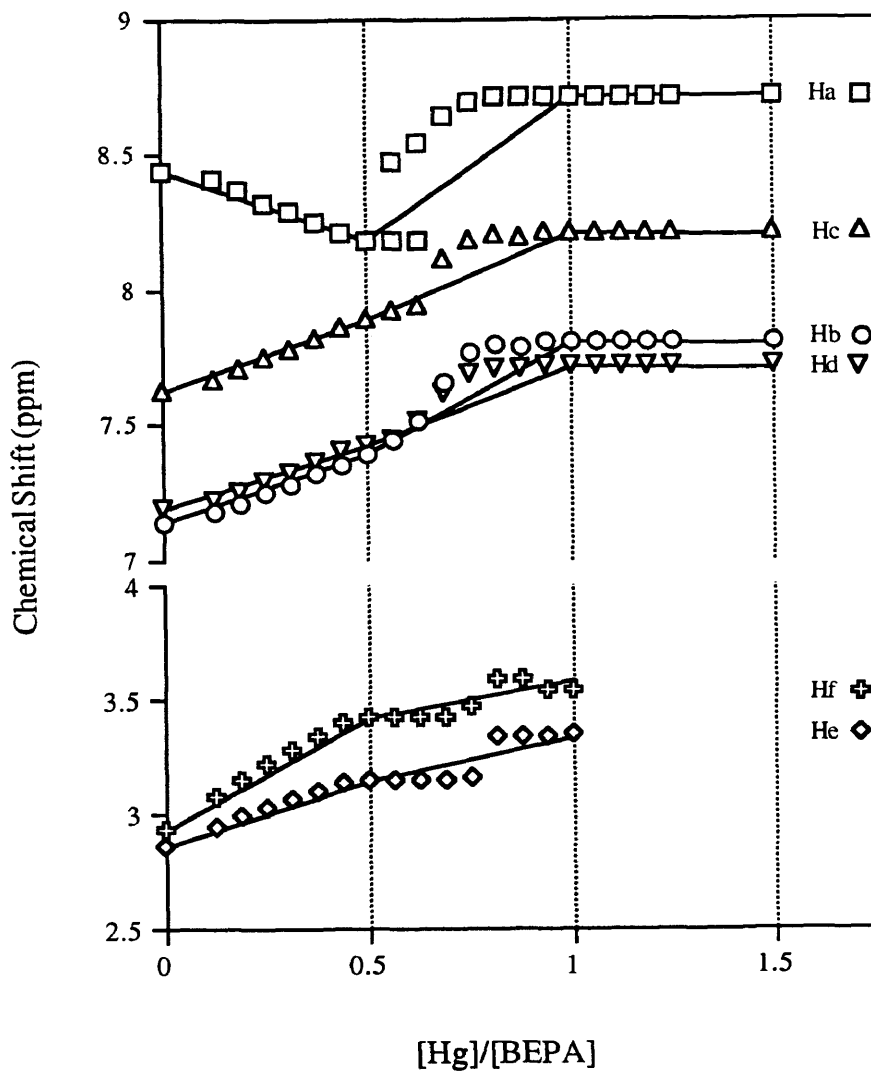


Figure 5. The chemical shifts of BEPA as a function of the $\text{Hg}(\text{ClO}_4)_2$ to BEPA ratio in CD_3CN at 20°C . The concentration of $\text{Hg}(\text{ClO}_4)_2$ was fixed at 2 mM. The lines represent the chemical shifts expected if the equilibrium constants for formation of $[\text{Hg}(\text{BEPA})_2]_2^{2+}$ and $[\text{Hg}(\text{BEPA})]^{2+}$ are large and there are no intervening complexes. A complex methylene environment precluded analysis of chemical shifts above 1.0 equivalents of $[\text{Hg}]/[\text{BEPA}]$.

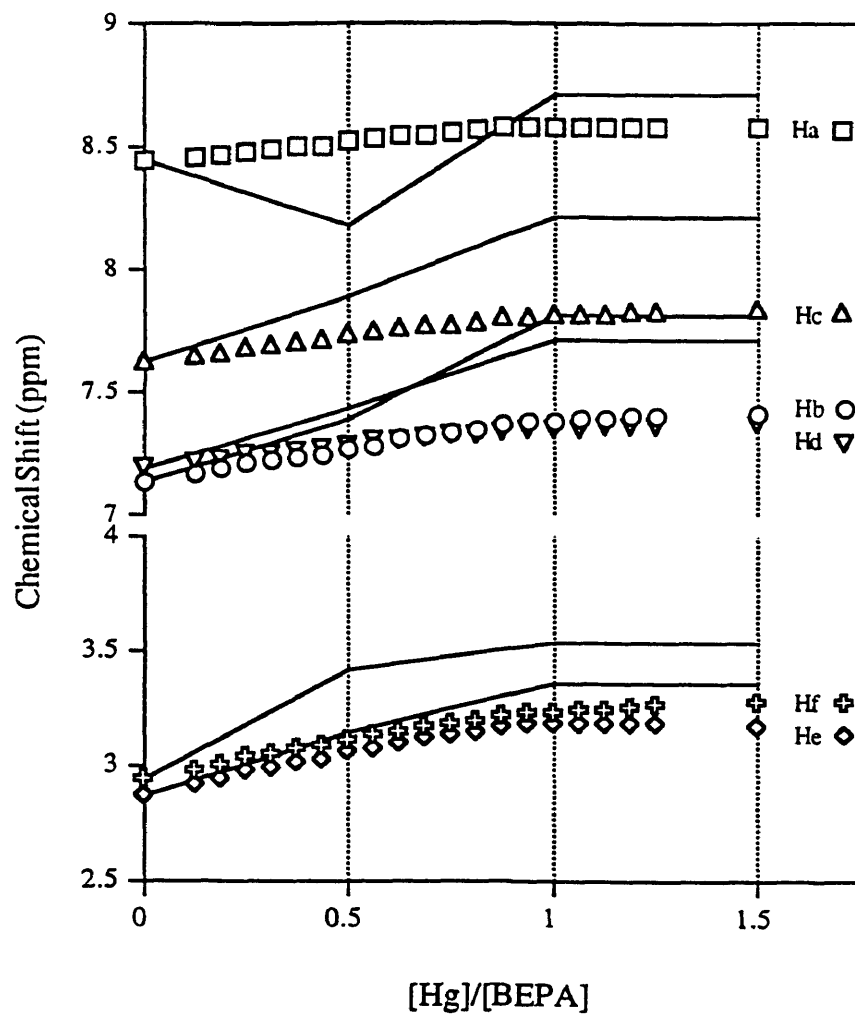


Figure 6. The chemical shifts of protons of BEPA as a function of the HgCl_2 to BEPA ratio in CD_3CN at 20°C . The concentration of HgCl_2 was fixed at 2 mM. The lines represent the chemical shifts expected if the equilibrium constant for formation of $[\text{Hg}(\text{BEPA})]^{2+}$ is large and there are no intervening complexes.

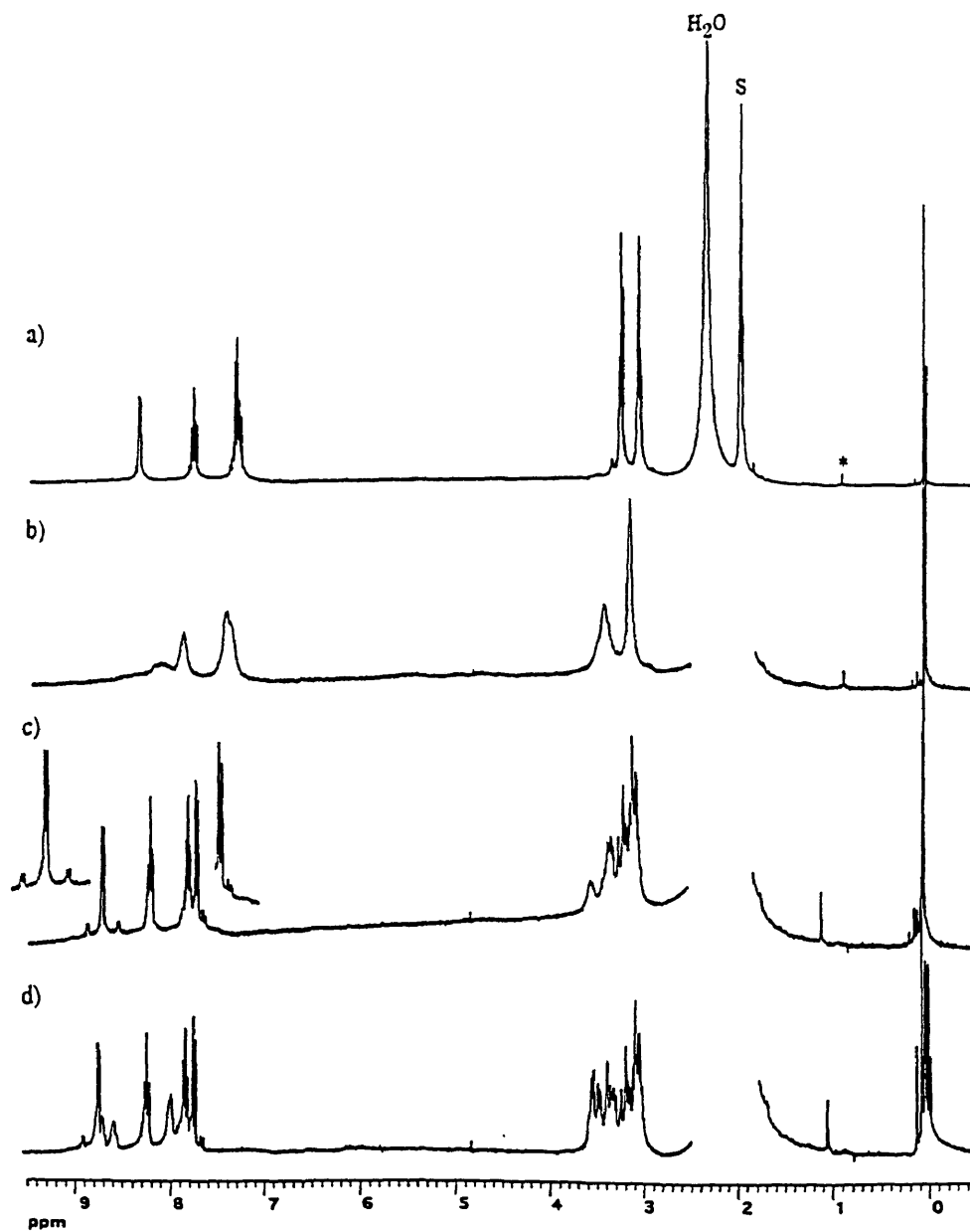


Figure 7 . Proton NMR spectra recorded at selected ratios of $\text{Hg}(\text{ClO}_4)_2$ to BEPA in CD_3CN at 20°C . The concentration of $\text{Hg}(\text{ClO}_4)_2$ was fixed at 2 mM. $[\text{Hg}(\text{ClO}_4)_2]/[\text{BEPA}] =$ a) 0.25, b) 0.5, c) 1.0, d) 1.5. S = CH_3CN ; * = impurity.

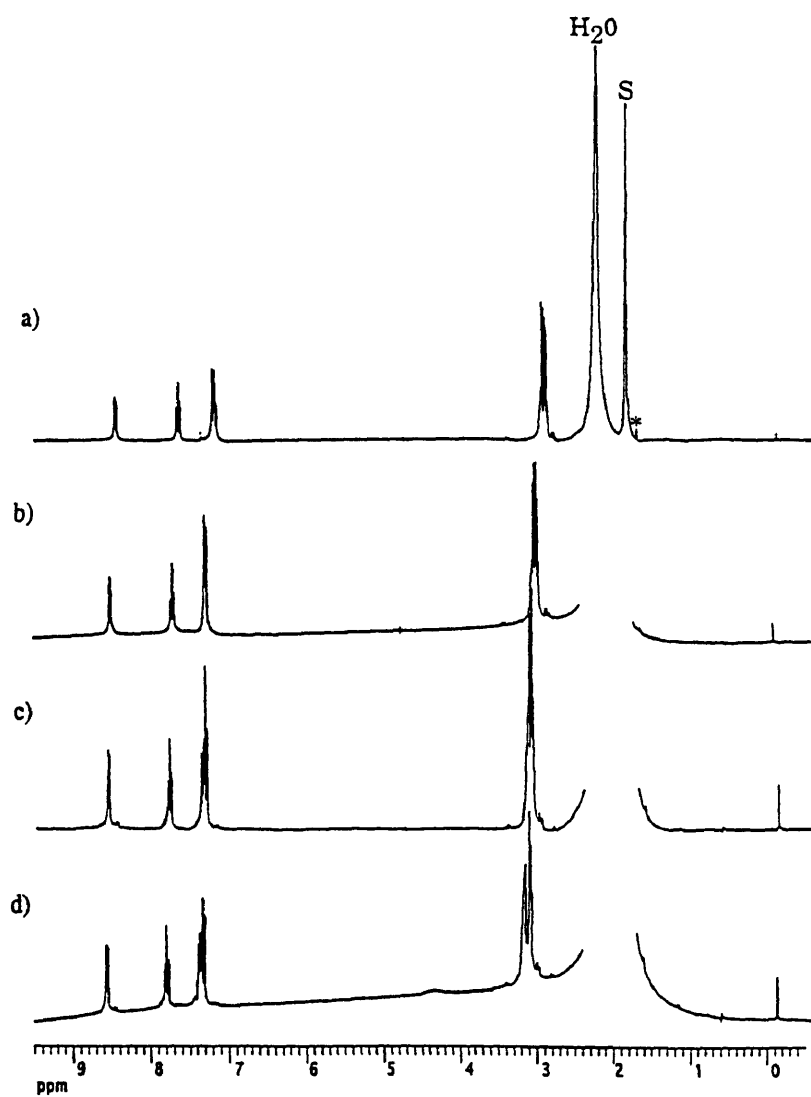


Figure 8. Proton NMR spectra recorded at selected ratios of HgCl_2 to BEPA in CD_3CN at 20°C . The concentration of HgCl_2 was fixed at 2 mM. $[\text{HgCl}_2]/[\text{BEPA}] =$ a) 0.25, b) 0.5, c) 1.0, d) 1.5. S = CH_3CN ; * = impurity.

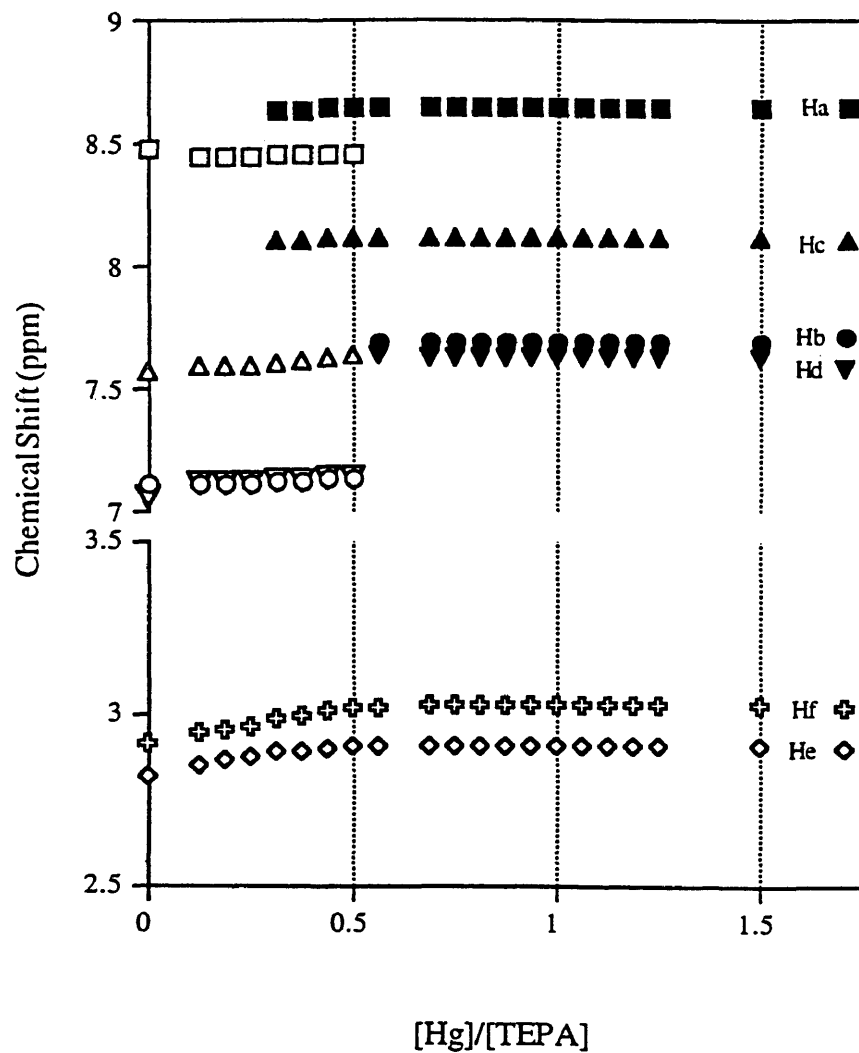


Figure 10. The chemical shifts of TEPA as a function of the $\text{Hg}(\text{ClO}_4)_2$ to TEPA ratio in CD_3CN at 20°C . The concentration of $\text{Hg}(\text{ClO}_4)_2$ was fixed at 2 mM. Open and shaded symbols correspond to two different ligand environments.

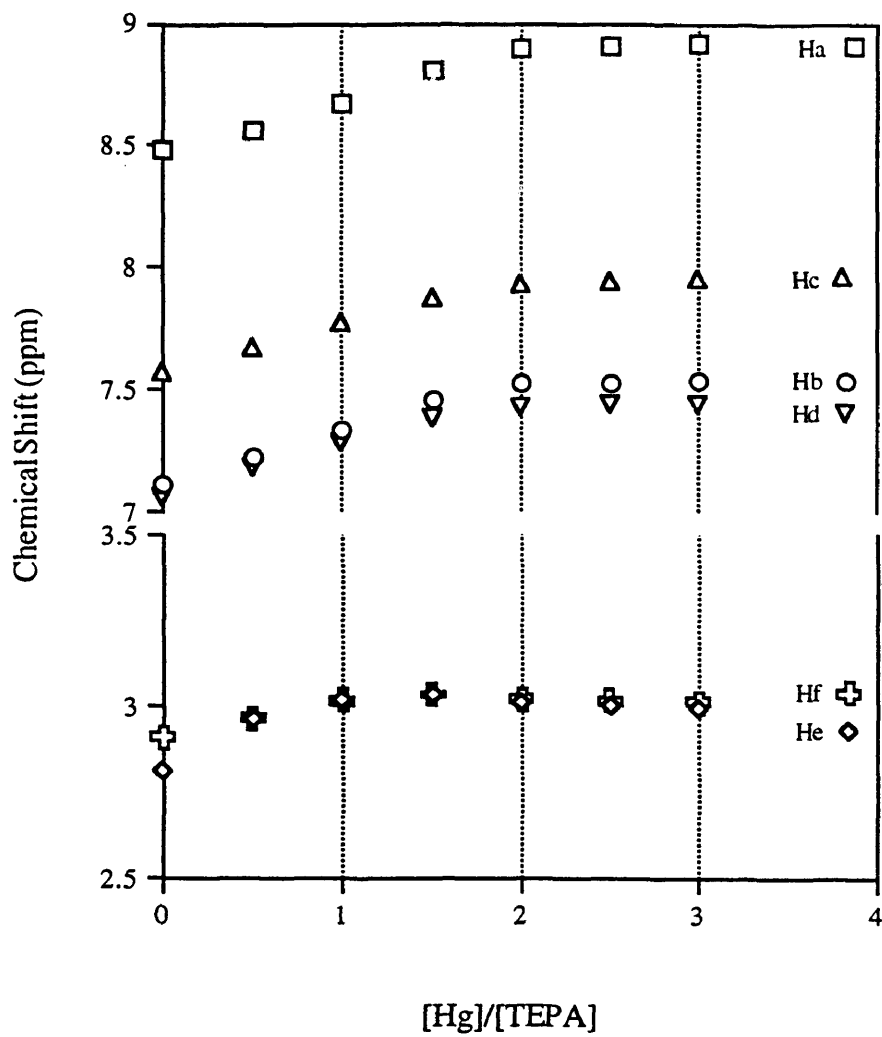


Figure 11. The chemical shifts of protons of TEPA as a function of the HgCl_2 to TEPA ratio in CD_3CN at 20°C . The concentration of HgCl_2 was fixed at 2 mM.

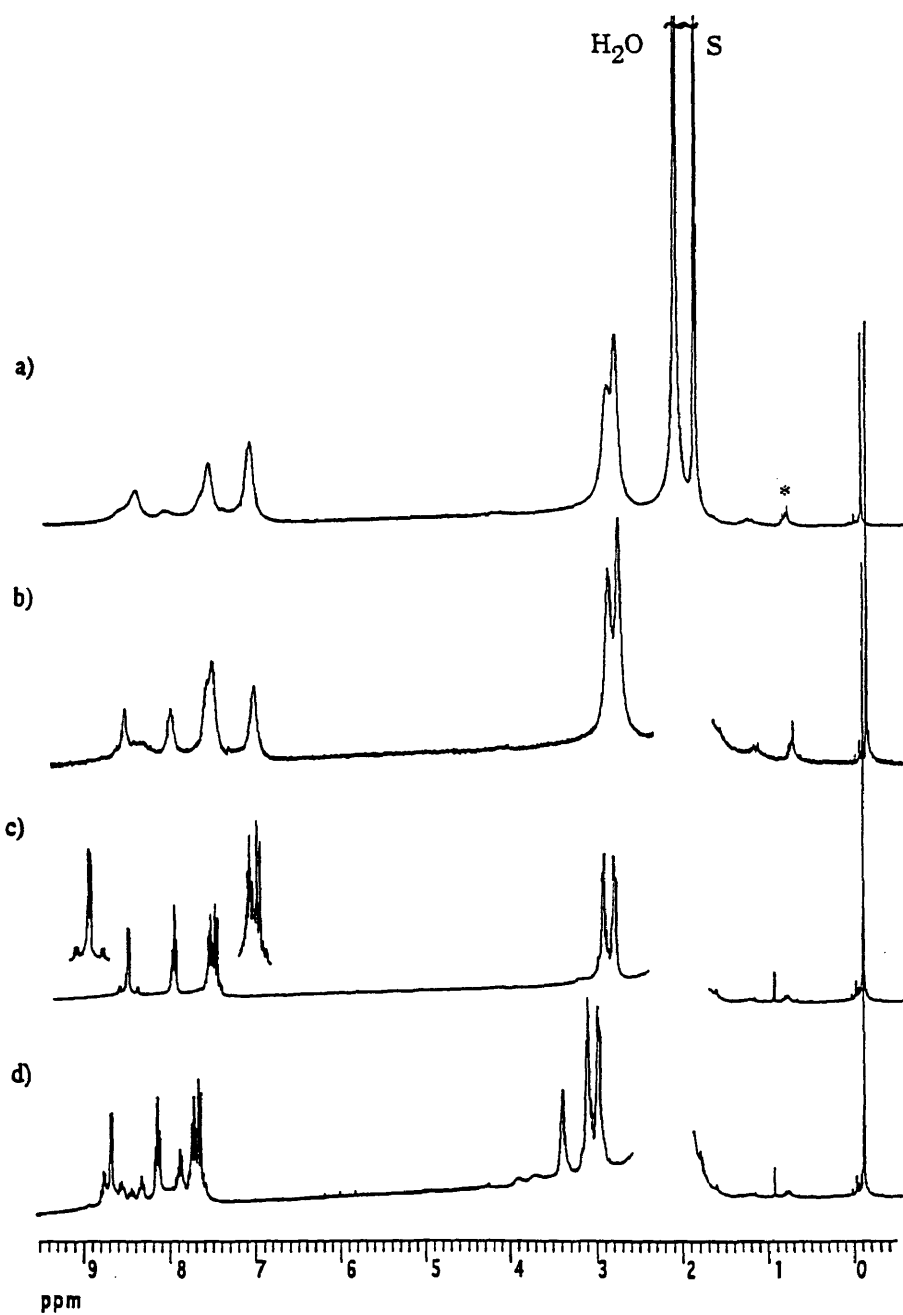


Figure 12. Proton NMR spectra recorded at selected ratios of $\text{Hg}(\text{ClO}_4)_2$ to TEPA in CD_3CN at 20°C . The concentration of $\text{Hg}(\text{ClO}_4)_2$ was fixed at 2 mM. $[\text{Hg}(\text{ClO}_4)_2]/[\text{TEPA}] =$ a) 0.25, b) 0.5, c) 1.0, d) 1.5. S = CH_3CN ; * = impurity.

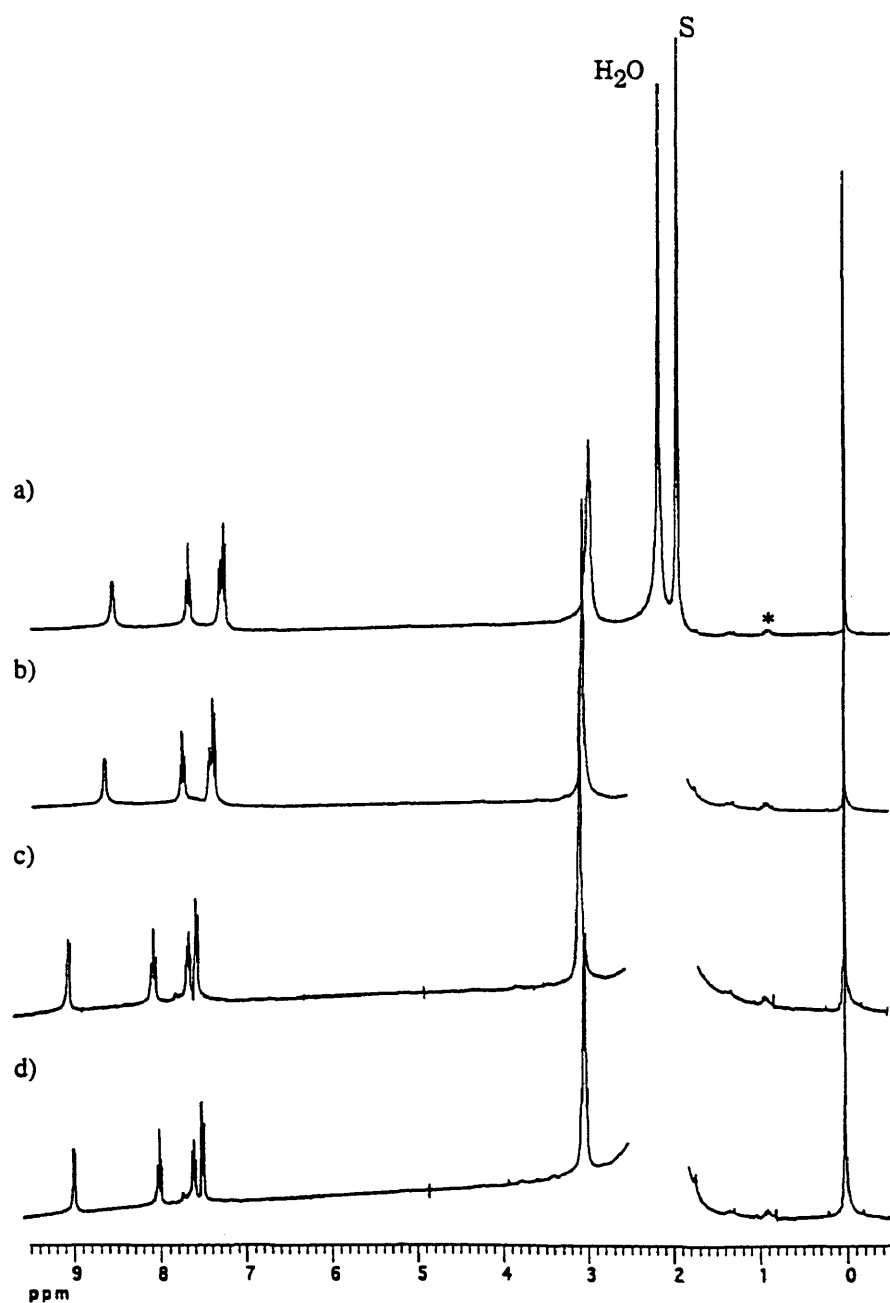


Figure 13. Proton NMR spectra recorded at selected ratios of HgCl₂ to TEPA in CD₃CN at 20° C. The concentration of HgCl₂ was fixed at 2 mM.

[HgCl₂]/[TEPA] = a) 0.50, b) 1.0, c) 2.0, d) 3.0. S = CH₃CN; * = impurity.

VITA

RACHEL E. FREER

The author was born in Cleveland, Ohio, on December 1, 1973. She graduated from Cleveland Heights High School in Cleveland, Ohio, in June of 1992, and The College of William and Mary in Williamsburg, Virginia, in May of 1996 with a B.S. degree in Chemistry.

After graduating with a M.A. degree in Chemistry, she will begin her career as a biologist with Syracuse Research Corporation in Arlington, Virginia.